

$P_c(4312)^+$, $P_c(4380)^+$, and $P_c(4457)^+$ as double triangle cuspsSatoshi X. Nakamura^{1,2,*}¹University of Science and Technology of China, Hefei 230026, People's Republic of China²State Key Laboratory of Particle Detection and Electronics (IHEP-USTC), Hefei 230036, People's Republic of China

Understanding the nature of the hidden charm pentaquark(like) signals in the LHCb data for $\Lambda_b^0 \rightarrow J/\psi p K^-$ is a central problem of hadron spectroscopy. We propose a scenario completely different from previous ones such as hadron molecules and compact pentaquarks. We identify relevant double triangle mechanisms with leading or lower-order singularities. The associated anomalous threshold cusps at the $\Sigma_c^{(*)}\bar{D}^{(*)}$ thresholds are significantly more singular than the ordinary ones. Then we demonstrate that the double triangle amplitudes reproduce the peak structures of $P_c(4312)^+$, $P_c(4380)^+$, and $P_c(4457)^+$ in the LHCb data, through an interference with other common mechanisms. Only the $P_c(4440)^+$ peak is due to a resonance with width and strength significantly smaller than previously estimated. P_c^+ signals are expected in other processes and the proposed model (partly) explains the current data such as: the GlueX J/ψ photoproduction data with no P_c^+ signals; the LHCb $\Lambda_b^0 \rightarrow J/\psi p \pi^-$ data with a possible signal only from $P_c(4440)^+$. The double triangle singularity is now a possible option to interpret resonancelike structures near thresholds in general.

I. INTRODUCTION

Hadron spectrum is a reflection of nonperturbative aspects of QCD. Exotic hadrons have structures different from the conventional quark-antiquark and three-quark [1], and are expected to provide a clue to assess a different aspect of QCD. Recent experimental discoveries of exotic hadron(like) signals are therefore exciting [2–9].

The LHCb Collaboration recently observed in $\Lambda_b^0 \rightarrow J/\psi p K^-$ three resonance(like) structures [10], interpreted as pentaquark states called $P_c(4312)^+$, $P_c(4440)^+$, and $P_c(4457)^+$, by updating their previous analysis [11]. Understanding the nature of the P_c^+ 's is certainly a central problem of the hadron spectroscopy. Because of the proximity of the P_c^+ masses to the $\Sigma_c(2455)\bar{D}^{(*)}$ thresholds¹, P_c^+ 's as $\Sigma_c(2455)\bar{D}^{(*)}$ molecules (bound states) may seem a natural interpretation of their identity [13–36]. Yet, constituent pentaquark pictures [37–44] and a hadrocharmonium [45] are also possible options. The LHCb data of the $J/\psi p$ invariant mass ($M_{J/\psi p}$) distribution has been analyzed with a K -matrix model that claimed a virtual state for $P_c(4312)^+$ [46]. Another analyses [34–36] based on one-pion-exchange plus contact interactions for the coupled $\Sigma_c^{(*)}\bar{D}^{(*)}$ system interpreted all the P_c^+ 's as $\Sigma_c^{(*)}\bar{D}^{(*)}$ bound states; they also claimed the existence of a narrow $P_c(4380)^+$ ². So far, all the models assigned a pole to each of the P_c^+ peaks³.

In order to establish P_c^+ 's as hadronic states, it is im-

portant to confirm their signals in other processes such as J/ψ photoproduction off a nucleon [48–54]. The GlueX Collaboration conducted such an experiment, finding no evidence [55]. This may indicate that the P_c^+ states couple weakly with a photon and could be seen in higher statistics data. Another possibility is that the P_c^+ peaks in $\Lambda_b^0 \rightarrow J/\psi p K^-$ are caused by kinematical effects such as threshold cusp and triangle singularity (TS) [56], and do not appear in the photoproduction; however, no relevant mechanism has been found. TS [57, 58] proposed for the previous P_c^+ [11] no longer fit the updated P_c^+ signals unless a pole is included [10].

In this work, we point out that a double triangle (DT) diagram [Fig. 1(a)] creates a kinematical effect that has not been explored for interpreting resonancelike structures. The effect is caused by the fact that each loop hits a TS and that the two TS can even occur almost simultaneously (leading singularity [59]). The associated anomalous threshold cusps are significantly more singular than the ordinary ones and, thus, can be a new option to understand exotic hadronlike signals near thresholds. We then demonstrate that the DT amplitudes reproduce the peak structures of $P_c(4312)^+$, $P_c(4380)^+$, and $P_c(4457)^+$ in the LHCb data, through an interference with other common mechanisms [Figs. 1(b) and 1(d)]. The LHCb data requires this proposed model to have only $P_c(4440)^+$ as a resonance with width and strength significantly smaller than previously estimated. The model can also (partly) explain P_c^+ signals in other data such as: no P_c^+ signals in the J/ψ photoproduction; $\Lambda_b^0 \rightarrow J/\psi p \pi^-$ data [60] suggesting only a $P_c(4440)^+$ signal. In this way, we bring a completely new understanding of the P_c^+ structures in the LHCb data.

* satoshi@ustc.edu.cn

¹ We follow the hadron naming scheme of [12]. For simplicity, however, we often denote $\Sigma_c(2455)^{+(++)}$, $\Sigma_c(2520)^{+(++)}$, $\Lambda_c(2595)^+$, $\Lambda_c(2625)^+$, and J/ψ by Σ_c , Σ_c^* , Λ_c^* , Λ_c^{**} , and ψ , respectively. $\Lambda_c^{(**)}$ and $\Sigma_c^{(*)}$ are also collectively denoted by Y_c . Charge indices are often suppressed.

² In this paper, $P_c(4380)^+$ does not refer to a broad state [11].

³ Although a K -matrix analysis [47] claimed $P_c(4457)^+$ as a threshold cusp, we put the conclusion on hold for insufficient

quality of fitting the $P_c(4312)^+$ peak and $\Sigma_c(2520)\bar{D}$ threshold region.

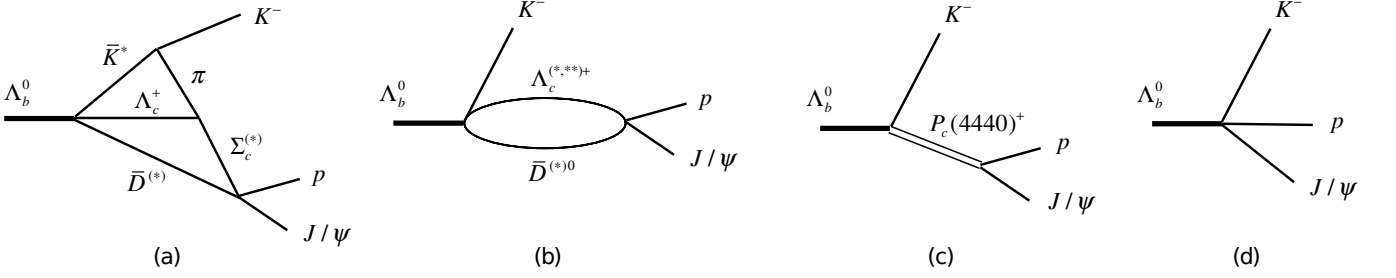


FIG. 1. $\Lambda_b^0 \rightarrow J/\psi p K^-$ mechanisms: (a) double triangle; (b) one-loop; (c) $P_c(4440)^+$ -excitation; (d) direct decay.

II. MODEL

Our model for $\Lambda_b^0 \rightarrow J/\psi p K^-$ is diagrammatically represented in Fig. 1. For loop diagrams of Fig. 1(a,b), we assume that color-favored $\Lambda_b^0 \rightarrow \Lambda_c^{(*)+} \bar{D}^{(*)} \bar{K}^{(*)}$ decays dominate over color-suppressed ones. We do not include color-suppressed $\Lambda_b^0 \rightarrow \Sigma_c^{(*)} \bar{D}^{(*)} K^-$ vertices that previous models often used with a possible problem of explaining P_c^+ production rates [26]. We could include color-suppressed processes since their suppression is generally difficult to predict [35] and the DT amplitudes might be more suppressed. We still take this assumption because the DT amplitudes are actually not significantly suppressed and, for fitting only the $M_{J/\psi p}$ distribution data, color-suppressed contributions are redundant and would not significantly improve the fit. Regarding the parity, we consider only parity-conserving mechanisms; parity-violating mechanisms should exist but are redundant in the fits. Partial waves of $J^P = 1/2^-, 3/2^-, 1/2^+$, and $3/2^+$ are considered; J^P denotes the spin-parity of $J/\psi p$.

We present amplitude formulas for representative diagrams in Fig. 1; see the Supplemental material for complete formulas and parameter values. We use the particle mass and width values from [12], and denote the energy, width, momentum, and polarization vector of a particle x by E_x , Γ_x , \mathbf{p}_x , and $\boldsymbol{\epsilon}_x$, respectively. We also denote a baryon(B)-meson(M) pair by $BM(J^P)$. A DT diagram [Fig. 1(a)] that includes $\Sigma_c \bar{D} (1/2^-)$ consists of four vertices such as $\Lambda_b^0 \rightarrow \Lambda_c^+ \bar{D} \bar{K}^*$, $\bar{K}^* \rightarrow \bar{K} \pi$, $\Lambda_c^+ \pi \rightarrow \Sigma_c$, and $\Sigma_c \bar{D} (1/2^-) \rightarrow J/\psi p$ given by

$$c_{\Lambda_c \bar{D} \bar{K}^*, \Lambda_b} \left(\frac{1}{2} t_{\bar{D}} \frac{1}{2} t_{\bar{K}^*} \middle| 00 \right) \boldsymbol{\sigma} \cdot \boldsymbol{\epsilon}_{\bar{K}^*} F_{\bar{K}^* \bar{D} \Lambda_c, \Lambda_b}^{00}, \quad (1)$$

$$c_{\bar{K} \pi, \bar{K}^*} \left(1 t_{\pi} \frac{1}{2} t_{\bar{K}} \middle| \frac{1}{2} t_{\bar{K}^*} \right) \boldsymbol{\epsilon}_{\bar{K}^*} \cdot (\mathbf{p}_{\bar{K}} - \mathbf{p}_{\pi}) f_{\bar{K} \pi, \bar{K}^*}^1, \quad (2)$$

$$c_{\Lambda_c \pi, \Sigma_c} \boldsymbol{\sigma} \cdot \mathbf{p}_{\pi} f_{\Lambda_c \pi, \Sigma_c}^1, \quad (3)$$

$$c_{\psi p, \Sigma_c \bar{D}}^{1/2^-} \left(1 t_{\Sigma_c} \frac{1}{2} t_{\bar{D}} \middle| \frac{1}{2} t_p \right) \boldsymbol{\sigma} \cdot \boldsymbol{\epsilon}_{\psi} f_{\psi p}^0 f_{\Sigma_c \bar{D}}^0, \quad (4)$$

respectively. Dipole form factors with a cutoff Λ are denoted by $F_{ijk,l}^{LL}$, f_{ij}^L , and $f_{ij,k}^L$. The parentheses are isospin Clebsch-Gordan coefficients (CGCs) with t_x being the isospin z -component of x . In Eq. (1) and later in

Eq. (6), the isospin of the $\bar{D}^{(*)} \bar{K}^{(*)}$ pair is 0 for assuming the color-favored Λ_b^0 decays. The couplings $c_{\bar{K} \pi, \bar{K}^*}$ and $c_{\Lambda_c \pi, \Sigma_c}$ are determined by the K^* and $\Sigma_c(2455)$ decay widths. The DT amplitude is

$$A_{\Sigma_c \bar{D} (1/2^-)}^{\text{DT}} = \sum_{\text{charge}} c_{\psi p, \Sigma_c \bar{D}}^{1/2^-} c_{\Lambda_c \pi, \Sigma_c} c_{\bar{K} \pi, \bar{K}^*} c_{\Lambda_c \bar{D} \bar{K}^*, \Lambda_b} \\ \times (\text{isospin CGCs}) \int d^3 p_{\pi} \int d^3 p_{\bar{D}} \\ \times \frac{\boldsymbol{\sigma} \cdot \boldsymbol{\epsilon}_{\psi} \boldsymbol{\sigma} \cdot \mathbf{p}_{\pi}}{E - E_{\bar{K}} - E_{\Sigma_c} - E_{\bar{D}} + \frac{i}{2} \Gamma_{\Sigma_c}} \\ \times \frac{\boldsymbol{\sigma} \cdot (\mathbf{p}_{\bar{K}} - \mathbf{p}_{\pi})}{E - E_{\bar{K}} - E_{\pi} - E_{\Lambda_c} - E_{\bar{D}} + i\epsilon} \\ \times \frac{f_{\psi p}^0 f_{\Sigma_c \bar{D}}^0 f_{\Lambda_c \pi, \Sigma_c}^1 f_{\bar{K} \pi, \bar{K}^*}^1 F_{\bar{K}^* \bar{D} \Lambda_c, \Lambda_b}^{00}}{E - E_{\bar{K}^*} - E_{\Lambda_c} - E_{\bar{D}} + \frac{i}{2} \Gamma_{\bar{K}^*}}, \quad (5)$$

where different charge states in the loops are summed with charge dependent particle masses; E is the total energy. The amplitude is implicitly sandwiched by initial Λ_b^0 and final p spin states.

The $\Lambda_c^+ \bar{D}^{*0} (1/2^-)$ one-loop amplitude [Fig. 1(b)] is composed by an initial $\Lambda_b^0 \rightarrow \Lambda_c^+ \bar{D}^{*0} K^-$ vertex

$$c_{\Lambda_c \bar{D}^* \bar{K}, \Lambda_b} \left(\frac{1}{2} t_{\bar{D}^*} \frac{1}{2} t_{\bar{K}} \middle| 00 \right) \boldsymbol{\sigma} \cdot \boldsymbol{\epsilon}_{\bar{D}^*} F_{\bar{K} \bar{D}^* \Lambda_c, \Lambda_b}^{00}, \quad (6)$$

and the subsequent $\Lambda_c^+ \bar{D}^{*0} (1/2^-) \rightarrow J/\psi p$ interaction

$$c_{\psi p, \Lambda_c \bar{D}^*}^{1/2^-} \boldsymbol{\sigma} \cdot \boldsymbol{\epsilon}_{\psi} \boldsymbol{\sigma} \cdot \boldsymbol{\epsilon}_{\bar{D}^*} f_{\psi p}^0 f_{\Lambda_c \bar{D}^*}^0. \quad (7)$$

The one-loop amplitude is

$$A_{\Lambda_c \bar{D}^*}^{\text{1L}} = 3 c_{\psi p, \Lambda_c \bar{D}^*}^{1/2^-} c_{\Lambda_c \bar{D}^* \bar{K}, \Lambda_b} \left(\frac{1}{2} t_{\bar{D}^*} \frac{1}{2} t_{\bar{K}} \middle| 00 \right) \boldsymbol{\sigma} \cdot \boldsymbol{\epsilon}_{\psi} \\ \times \int d^3 p_{\bar{D}^*} \frac{f_{\psi p}^0 f_{\Lambda_c \bar{D}^*}^0 F_{\bar{K} \bar{D}^* \Lambda_c, \Lambda_b}^{00}}{E - E_{\bar{K}} - E_{\Lambda_c} - E_{\bar{D}^*} + \frac{i}{2} \Gamma_{\bar{D}^*}}, \quad (8)$$

with $\Gamma_{\bar{D}^*0} = 55$ keV [61].

The $P_c(4440)^+$ amplitude [Fig. 1(c)] is given in the Breit-Wigner form with adjustable $P_c(4440)^+$ mass, width, and coupling. For J^P of $P_c(4440)^+$, we examine $1/2^{\pm}$ and $3/2^{\pm}$ cases. The internal structure of $P_c(4440)^+$ is beyond the scope of this work. We also consider a direct decay mechanism [Fig. 1(d)] in each

partial wave with a real coupling strength. This simulates all mechanisms not belonging to the diagrams of Figs. 1(a)-1(c).

The $Y_c \bar{D}^{(*)}$ pairs in the DT and one-loop diagrams require a nonperturbative treatment. Meanwhile, the lattice QCD [62] found a weak $J/\psi p \rightarrow J/\psi p$ interaction. Thus, a reasonable approach is to develop a $Y_c \bar{D}^{(*)}$ coupled-channel model incorporating the heavy quark spin symmetry [28, 34–36]. However, we take a simpler approach and use a single-channel contact interaction model [63] to calculate a $Y_c \bar{D}^{(*)}$ scattering amplitude that maintains only the elastic unitarity. Then, a perturbative transition to $J/\psi p$ follows. The resulting $Y_c \bar{D}^{(*)} \rightarrow J/\psi p$ amplitude is implemented in Eqs. (5) and (8); see the Supplemental material. Other possible coupled-channel effects are assumed to be absorbed by complex couplings fitted to the data. This simplification can be justified for the limited purpose of proposing a new scenario for the P_c^+ structures in the LHCb data. Within our model, the P_c^+ structures (except for $P_c(4440)^+$) are mostly described by the kinematical effects, and not directly by poles from the $Y_c \bar{D}^{(*)}$ scattering. Therefore, the data can only loosely constrain our $Y_c \bar{D}^{(*)}$ interactions. Conversely, the details of the $Y_c \bar{D}^{(*)}$ scattering do not play a major role. This is in contrast with hadron-molecule models for which the $Y_c \bar{D}^{(*)}$ interactions must be fine-tuned to get poles at right positions; the details do matter.

III. RESULTS

A. Double triangle amplitudes and their singular behaviors

The DT amplitudes cause the leading and lower-order singularities (or anomalous thresholds) [59] when Σ_c and Σ_c^* propagates in Fig. 1(a), respectively. This is analogous to a single triangle diagram causing TS as its leading singularity. According to the Coleman-Norton theorem [64], the leading singularity occurs when a given loop process is kinematically allowed at the classical level. The lower-order singularity occurs when one (or more) of the intermediate states is necessarily off-shell. Details on the kinematical conditions are given in the Supplemental material. As a TS-enhanced amplitude shows a logarithmically singular behavior, the DT leading and lower-order singularities generate their own singular behaviors. While the singular behaviors can, in principle, be examined by analyzing the corresponding Landau equations [59, 65], we study them numerically below.

We plot in Fig. 2(a,b) the DT amplitude that includes $\Sigma_c^+ \bar{D}^0 (1/2^-)$ [red solid curves]. A singular behavior clearly shows up near the $\Sigma_c^+ \bar{D}^0$ threshold. We also plot a threshold cusp, due to the square-root singularity, from a $\Sigma_c^+ \bar{D}^0$ one-loop amplitude similar to Fig. 1(b) [green dotted curves]; the imaginary part does not vanish below the threshold for $\Gamma_{\Sigma_c^+} \neq 0$. The DT cusp due to

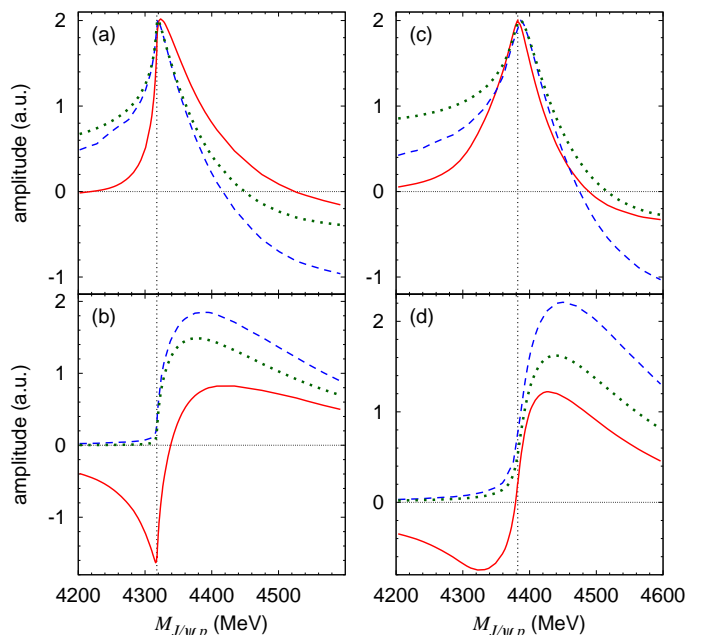


FIG. 2. Double triangle amplitudes. The panel (a) [(b)] shows the real [imaginary] part. The red solid curves are for $\Sigma_c^{(*)} \bar{D}^{(*)} = \Sigma_c^+ \bar{D}^0$ in Fig. 1(a) [$\Lambda = 1$ GeV; perturbative $\Sigma_c^{(*)} \bar{D}^{(*)} \rightarrow J/\psi p$]. They reduce to the blue dashed ones by using $m_{\Lambda_c^+} = 3$ GeV. The green dotted curves are the $\Sigma_c^+ \bar{D}^0$ one-loop amplitude. All the amplitudes are normalized so that the real parts have the same peak height. The dotted vertical lines indicate the $\Sigma_c^+ \bar{D}^0$ thresholds. The amplitudes shown in the panel (c) [(d)] are obtained from those in (a) [(b)] by replacing Σ_c^+ with Σ_c^{*+} .

the leading singularity is clearly more singular. For an illustration, we replace the Λ_c^+ mass in the DT amplitude with a hypothetically heavy value (3 GeV) so that the loop integral can hit only the $\Sigma_c^+ \bar{D}^0$ threshold singularity. The resultant amplitude [blue dashed curves] behaves like an ordinary threshold cusp. The amplitudes shown in Fig. 2(a,b) include $\Sigma_c^+ \bar{D}^0 \rightarrow J/\psi p$ treated as the first-order perturbation. A non-perturbative attractive $\Sigma_c^+ \bar{D}^0$ interaction significantly enhances the singular behaviors [66]. Similar plots in Fig. 2(c,d) are obtained by replacing Σ_c^+ in the amplitudes shown in Fig. 2(a,b) with Σ_c^{*+} . While this DT amplitude with $\Sigma_c^{*+} \bar{D}^0$ has the lower-order singularity and is more singular than the ordinary threshold cusp, it is less singular than the DT amplitude with $\Sigma_c^+ \bar{D}^0$ having the leading singularity.

To clarify that the DT amplitudes and ordinary threshold cusps have different singular behaviors, we divide the former by the latter and show the ratios in Fig. 3. The singular behaviors still remain in the real part of the ratios. The first [second] derivative of the ratio in Fig. 3(a) [3(b)] seems divergent at the $\Sigma_c^+ \bar{D}^0$ [$\Sigma_c^{*+} \bar{D}^0$] threshold, showing a qualitative difference between the leading and lower-order singularities. The results in Figs. 2-3 indicate that, in general, the DT cusp might be an option to

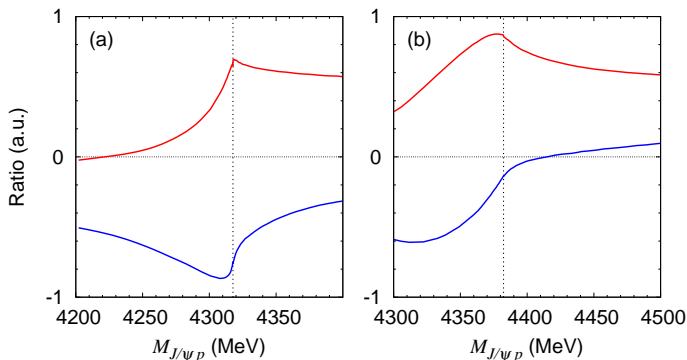


FIG. 3. Ratio of double triangle (A_{DT}) to one-loop ($A_{1\text{L}}$) amplitudes. The ratio in the panel (a) [(b)] is from the amplitudes including $\Sigma_c^+ \bar{D}^0$ [$\Sigma_c^{*+} \bar{D}^0$] intermediate states. The upper red (lower blue) curves show $\text{Re}[A_{\text{DT}}/A_{1\text{L}}]$ ($\text{Im}[A_{\text{DT}}/A_{1\text{L}}]$). The dotted vertical lines in the panel (a) [(b)] indicate the $\Sigma_c^+ \bar{D}^0$ [$\Sigma_c^{*+} \bar{D}^0$] threshold.

understand resonancelike structures near thresholds.

As expected from Fig. 2, the DT amplitude alone creates a peak at the $\Sigma_c^{(*)} \bar{D}^{(*)}$ threshold in the $M_{J/\psi p}$ distribution of $\Lambda_b^0 \rightarrow J/\psi p K^-$. This peak cannot be identified with a P_c^+ peak which is located slightly below the threshold. However, suppose there exists a smooth amplitude that interferes with the real (imaginary) part of the DT amplitude of Fig. 2 destructively (constructively) near the threshold. This coherent sum generates a peak slightly below the $\Sigma_c^{(*)} \bar{D}^{(*)}$ threshold. This is how the P_c^+ -like structures (other than $P_c(4440)^+$) show up from the DT mechanisms.

B. Analysis of the LHCb data

For describing $\Lambda_b^0 \rightarrow J/\psi p K^-$, our full model includes: (i) DT mechanisms with $\Sigma_c(2455) \bar{D}(1/2^-)$, $\Sigma_c(2520) \bar{D}(3/2^-)$, $\Sigma_c(2455) \bar{D}^*(1/2^-)$, $\Sigma_c(2455) \bar{D}^*(3/2^-)$, $\Sigma_c(2520) \bar{D}^*(1/2^-)$, and $\Sigma_c(2520) \bar{D}^*(3/2^-)$; (ii) one-loop mechanisms with $\Lambda_c^+ \bar{D}^{*0}(1/2^-)$, $\Lambda_c(2595)^+ \bar{D}^0(1/2^+)$, and $\Lambda_c(2625)^+ \bar{D}^0(3/2^+)$; (iii) $P_c(4440)^+$ mechanism; (iv) direct decay mechanisms. Regarding the number of fitting parameters, each mechanism in the items (i)-(iii) has an adjustable complex overall factor to fit the data; 2×10 parameters. Each direct decay mechanism (iv) has a real coupling strength; 4 parameters. The $P_c(4440)^+$ mass and width are adjustable. We also adjust a repulsive $\Lambda_c^+ \bar{D}^{*0}$ interaction strength. Because the overall absolute normalization of the full amplitude is arbitrary, we have totally 26 parameters. Although the heavy quark spin symmetry may constrain the parameters, we adjust them rather freely in the fits. This can be justified because the fitting parameters can effectively absorb effects from mechanisms not explicitly considered such

as parity-violating amplitudes; more discussions in the Supplemental material.

Regarding the elastic $Y_c \bar{D}^{(*)}$ interaction strengths, we examine if the fit favors an attractive or repulsive interaction for a given BM (J^P). The fit favors attractions for $\Sigma_c(2455) \bar{D}(1/2^-)$, $\Sigma_c(2520) \bar{D}(3/2^-)$, $\Sigma_c(2455) \bar{D}^*(1/2^-)$, $\Sigma_c(2455) \bar{D}^*(3/2^-)$, $\Lambda_c(2595)^+ \bar{D}^0(1/2^+)$, $\Lambda_c(2625)^+ \bar{D}^0(3/2^+)$, and repulsions for $\Sigma_c(2520) \bar{D}^*(1/2^-)$, $\Sigma_c(2520) \bar{D}^*(3/2^-)$, $\Lambda_c^+ \bar{D}^{*0}(1/2^-)$. Then we fix the coupling strength so that the scattering length is $a \sim 0.5$ fm⁴ for the attraction. The repulsive $\Lambda_c^+ \bar{D}^{*0}(1/2^-)$ interaction strength is fitted to the data because the fit quality is rather sensitive; $a \sim -0.4, -0.2$, and -0.05 fm for $\Lambda \sim 0.8, 1$, and 1.5 – 2 GeV, respectively. The other repulsive interactions have the same strength as $\Lambda_c^+ \bar{D}^{*0}$. It is noted that, within our model, spectrum peak positions are not very sensitive to the a values. The cutoff in the form factors is fixed at $\Lambda = 1$ GeV unless otherwise stated. Only the direct decay amplitudes include different cutoffs on $p_{\bar{K}}$ so that their $M_{J/\psi p}$ distribution is similar to the phase-space shape.

We compare our calculation with the LHCb data [10] in Fig. 4(a). The experimental resolution is considered in the calculation. Our full model (red solid curve) well fits the data. The $P_c(4312)^+$, $P_c(4380)^+$, and $P_c(4457)^+$ peaks are well described by the kinematical effects from the considered mechanisms, and not by poles near the peak positions. Only the $P_c(4440)^+$ peak requires a resonance pole for which we choose $J^P = 3/2^-$ in the figure. The fit quality does not significantly change when varying the cutoff over $\Lambda = 0.8$ – 2 GeV and when choosing $J^P = 1/2^\pm$ and $3/2^\pm$ for $P_c(4440)^+$; the fits thus do not favor a particular J^P of $P_c(4440)^+$. We simplify the model by omitting the $1/2^+$ and $3/2^+$ amplitudes, and treating $Y_c \bar{D}^{(*)} \rightarrow J/\psi p$ perturbatively. With 19 parameters to refit, main features of the data are fairly well captured (blue dashed curve). Still, the structures are less sharp near the thresholds because of lacking the strong $Y_c \bar{D}^{(*)}$ scattering. The $1/2^+$ and $3/2^+$ amplitudes are also needed for a more precise fit.

In Fig. 4(b), we show the full model's partial wave contributions that do not interfere with each other in the $M_{J/\psi p}$ distribution. In the $1/2^-$ (magenta dashed curve) and $3/2^-$ (blue dotted curve) contributions, the interference between the DT and direct decay mechanisms creates bumps slightly below the $\Sigma_c^{(*)} \bar{D}^{(*)}$ thresholds where the $P_c(4312)^+$, $P_c(4380)^+$, and $P_c(4457)^+$ peaks are located. The $1/2^-$ contribution also shows a bent due to the $\Lambda_c^+ \bar{D}^{*0}$ threshold cusp, being consistent with the data. The $1/2^+$ (green dash-dotted curve) and $3/2^+$ (brown dash-two-dotted curve) contributions exhibit $\Lambda_c(2595)^+ \bar{D}^0$ and $\Lambda_c(2625)^+ \bar{D}^0$ threshold cusps, respectively, capturing the characteristic structures in

⁴ The scattering length (a) is related to the phase shift (δ) by $p \cot \delta = 1/a + \mathcal{O}(p^2)$.

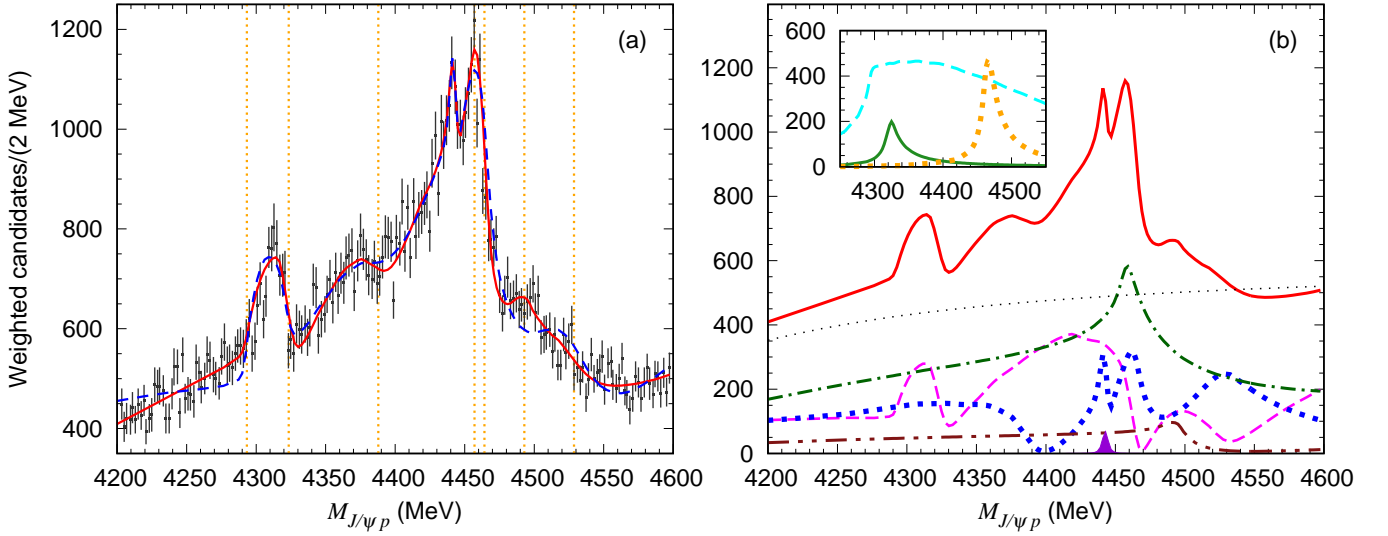


FIG. 4. $J/\psi p$ invariant mass ($M_{J/\psi p}$) distribution for $\Lambda_b^0 \rightarrow J/\psi p K^-$. (a) Comparison with the LHCb data ($\cos\theta_{P_c}$ -weighted samples) [10]. The red solid (blue dashed) curve is from the full (simplified) model; see the text for details on the models. The dotted vertical lines indicate thresholds for, from left to right, $\Lambda_c^+ \bar{D}^{*0}$, $\Sigma_c(2455)^{++} D^-$, $\Sigma_c(2520)^{++} D^-$, $\Lambda_c(2595)^+ \bar{D}^0$, $\Sigma_c(2455)^{++} D^{*-}$, $\Lambda_c(2625)^+ \bar{D}^0$, and $\Sigma_c(2520)^{++} D^{*-}$, respectively. (b) Partial wave contributions specified by J^P of the $J/\psi p$ pair. The magenta dashed, blue dotted, green dash-dotted, and brown dash-two-dotted curves are for $J^P = 1/2^-, 3/2^-, 1/2^+$, and $3/2^+$, respectively. The solid violet peak is the $P_c(4440)^+(3/2^-)$ contribution without interference. The thin black dotted curve is the sum of the direct decay mechanisms. The red solid curve is from the full model. In the insert, the green solid, orange dotted, and cyan dashed curves are contributions from the double triangle mechanism with $\Sigma_c \bar{D}(1/2^-)$, that with $\Sigma_c \bar{D}^*(1/2^-)$, and the $\Lambda_c^+ \bar{D}^{*0}(1/2^-)$ one-loop mechanism, respectively, without the interference.

the data. Although the $1/2^+$ peak seems a large contribution, this is due to a constructive interference between the $\Lambda_c(2595)^+ \bar{D}^0$ one-loop and direct decay amplitudes; the $\Lambda_c(2595)^+ \bar{D}^0$ one-loop amplitude itself is significantly smaller than the $\Lambda_c^+ \bar{D}^{*0}$ one-loop amplitude in magnitude. The sum of the direct decay mechanisms shows a phase-space-like distribution (thin black dotted curve). This partial wave decomposition would involve uncertainty due to the limited experimental information.

The $P_c(4440)^+(3/2^-)$ contribution without interference is shown in Fig. 4(b) [violet solid peak]. The mass and width from our fit is 4443.1 ± 1.4 MeV and 2.7 ± 2.4 MeV, respectively; the statistical errors are estimated just for a reference by varying only the $P_c(4440)^+$ mass, width, and coupling. The cutoff dependence is safely within the errors. Comparing with the LHCb analysis [10], $4440.3 \pm 1.3_{-4.7}^{+4.1}$ MeV and $20.6 \pm 4.9_{-10.1}^{+8.7}$ MeV, the width is significantly narrower. Also, the $P_c(4440)^+$ contribution is only $\sim 1/22$ of the LHCb's estimate: $\mathcal{R} \equiv \mathcal{B}(\Lambda_b^0 \rightarrow P_c^+ K^-) \mathcal{B}(P_c^+ \rightarrow J/\psi p) / \mathcal{B}(\Lambda_b^0 \rightarrow J/\psi p K^-) = 1.11 \pm 0.33_{-0.10}^{+0.22}$ %. This difference arises because the LHCb fitted the structure at $M_{J/\psi p} \sim 4450$ MeV with incoherent $P_c(4440)^+$ and $P_c(4457)^+$ contributions while we describe a large portion of the structure with the kinematical effects and attribute only the small spike to the $P_c(4440)^+$ and its interference.

The quality of the fit could be slightly improved with more attractive $\Sigma_c^{(*)} \bar{D}^{(*)}$ interactions. However, such in-

teractions generate virtual poles near the thresholds and, as a result, $\gamma p \rightarrow J/\psi p$ cross section would have sharp peaks at the $\Sigma_c^{(*)} \bar{D}^{(*)}$ thresholds. Since the GlueX did not find such peaks [55], we fix the $\Sigma_c^{(*)} \bar{D}^{(*)}$ interactions at the moderate strength so that no poles are generated close to the thresholds⁵.

To examine whether the DT amplitudes are significantly suppressed compared to other mechanisms, we show the DT and one-loop contributions to the $1/2^-$ partial wave in the insert of Fig. 4(b). The peak height of the DT contributions is comparable to that of the one-loop contribution. We can further compare the coupling strength of the DT amplitude [Eq. (5)] to that of the $\Lambda_c^+ \bar{D}^{*0}$ one-loop amplitude [Eq. (8)] by introducing a ratio:

$$R = \left| \frac{c_{\psi p, \Sigma_c \bar{D}}^{1/2^-} c_{\Lambda_c \bar{D} \bar{K}^*, \Lambda_b}}{c_{\psi p, \Lambda_c \bar{D}^*}^{1/2^-} c_{\Lambda_c \bar{D}^* \bar{K}, \Lambda_b}} \right|, \quad (9)$$

where well-controlled parameters ($c_{\bar{K} \pi, \bar{K}^*}$, $c_{\Lambda_c \pi, \Sigma_c}$) are excluded. Fitting the LHCb data gives $R = 7.2 - 3.2$ for $\Lambda = 0.8 - 2$ GeV. Thus, unreasonably large parameter values ($R \gg 1$) are not necessary, indicating that the

⁵ Our $\Sigma_c \bar{D}$ interaction model with $a \sim 0.5$ fm generates a virtual pole at ~ 20 MeV below the threshold.

comparable strengths of the DT and one-loop amplitudes are not an artifact.

Our model partly explains the absence of P_c^+ signals in J/ψ photoproduction data [55]. All P_c^+ peaks, except for $P_c(4440)^+$, in $\Lambda_b^0 \rightarrow J/\psi p K^-$ are caused by the kinematical effect (DT mechanisms and its interference) that requires an accompanying K^- in the final state. The $\gamma p \rightarrow J/\psi p$ process cannot accommodate this kinematical effect and, thus, has no P_c^+ signals. For $P_c(4440)^+$, its width and fit fraction from our analysis are significantly smaller than those from the LHCb's. In this case, observing a $P_c(4440)^+$ signal in J/ψ photoproduction would be more challenging than expected based on the LHCb result.

An evidence for P_c^+ was also found in $\Lambda_b^0 \rightarrow J/\psi p \pi^-$. The $M_{J/\psi p}$ distribution [Fig. 3(b) of [60]] seems that the $M_{J/\psi p}$ bin of $P_c(4440)^+$ is enhanced, whereas this is not the case for the other P_c^+ 's. This observation may conflict with some P_c^+ models but not ours because: the $P_c(4440)^+$ [DT] mechanisms in $\Lambda_b^0 \rightarrow J/\psi p K^-$ can [cannot] be shared by $\Lambda_b^0 \rightarrow J/\psi p \pi^-$ and, thus, only $P_c(4440)^+$ appears in the latter. For the limited statistics, P_c^+ signals in $\Lambda_b^0 \rightarrow J/\psi p \pi^-$ are still inconclusive. Higher statistics data can seriously test the models.

IV. SUMMARY AND FUTURE PERSPECTIVE

We analyzed the LHCb data for the $M_{J/\psi p}$ distribution of $\Lambda_b^0 \rightarrow J/\psi p K^-$. We found that the P_c^+ structures are well described by the double triangle cusps and their interference with the common mechanisms. Only $P_c(4440)^+$ is interpreted as a resonance but its width and strength are significantly smaller than the LHCb result. The analysis thus proposes an understanding of the P_c^+ peaks completely different from the previous ones such as hadron molecules and compact pentaquarks.

An interesting next step is to study $\Lambda_b^0 \rightarrow \Sigma_c^{(*)} \bar{D}^{(*)} K^-$. An immediate prediction is TS peaks at $M_{\Sigma_c K^-} \sim 3.40$ GeV and $M_{\Sigma_c^* K^-} \sim 3.21$ GeV due to a single triangle diagram obtained by removing $\Sigma_c^{(*)} \bar{D}^{(*)} \rightarrow J/\psi p$ vertex from Fig. 1(a). To examine the P_c^+ structures, a coupled-channel treatment of the $Y_c \bar{D}^{(*)}$ scattering is necessary. It is also interesting to understand other resonancelike structures near thresholds with DT cusps that should now be in the list of possible interpretations.

ACKNOWLEDGMENTS

I thank Feng-Kun Guo and Christoph Hanhart for useful discussions and comments on the manuscript. This work is in part supported by National Natural Science Foundation of China (NSFC) under contracts U2032103 and 11625523, and also by National Key Research and Development Program of China under Contracts 2020YFA0406400.

Supplemental material

1. $\Lambda_b^0 \rightarrow J/\psi p K^-$ amplitudes

We present formulas for diagrams of Fig. 1. For the present study, we consider only parity-conserving mechanisms. For double triangle (DT) diagrams of Fig. 1(a), we consider those including $\Sigma_c \bar{D}(1/2^-)$, $\Sigma_c^* \bar{D}(3/2^-)$, $\Sigma_c \bar{D}^*(1/2^-)$, $\Sigma_c \bar{D}^*(3/2^-)$, $\Sigma_c^* \bar{D}^*(1/2^-)$, and $\Sigma_c^* \bar{D}^*(3/2^-)$ pairs going to $J/\psi p$ [$\Sigma_c \equiv \Sigma_c(2455)^{+,++}$, $\Sigma_c^* \equiv \Sigma_c(2520)^{+,+++}$]. Each of the DT diagrams includes four vertices. The initial one is either $\Lambda_b^0 \rightarrow \Lambda_c^+ \bar{D} \bar{K}^*$ or $\Lambda_b^0 \rightarrow \Lambda_c^+ \bar{D}^* \bar{K}^*$ vertices given by

$$c_{\Lambda_c \bar{D} \bar{K}^*, \Lambda_b} \left(\frac{1}{2} t_{\bar{D}} \frac{1}{2} t_{\bar{K}^*} \middle| 00 \right) \boldsymbol{\sigma} \cdot \boldsymbol{\epsilon}_{\bar{K}^*} F_{\bar{K}^* \bar{D} \Lambda_c, \Lambda_b}^{00}, \quad (10)$$

$$c_{\Lambda_c \bar{D}^* \bar{K}^*, \Lambda_b} \left(\frac{1}{2} t_{\bar{D}^*} \frac{1}{2} t_{\bar{K}^*} \middle| 00 \right) i \boldsymbol{\sigma} \cdot (\boldsymbol{\epsilon}_{\bar{K}^*} \times \boldsymbol{\epsilon}_{\bar{D}^*}) F_{\bar{K}^* \bar{D}^* \Lambda_c, \Lambda_b}^{00}, \quad (11)$$

respectively, where the coupling constants $c_{\Lambda_c \bar{D} \bar{K}^*, \Lambda_b}$ and $c_{\Lambda_c \bar{D}^* \bar{K}^*, \Lambda_b}$ are generally complex values. Here and later in Eqs. (29)-(31), we assume that color-favored Λ_b^0 decays [Fig. 4(a)] dominate over color-suppressed ones [Fig. 4(b)], and thus the isospin of the $\bar{D}^{(*)} \bar{K}^{(*)}$ pair is 0. We have used dipole form factors $F_{ij,k,l}^{LL'}$ given as

$$F_{ij,k,l}^{LL'} = \frac{1}{\sqrt{E_i E_j E_k E_l}} \left(\frac{\Lambda^2}{\Lambda^2 + q_{ij}^2} \right)^{2+\frac{L}{2}} \left(\frac{\Lambda'^2}{\Lambda'^2 + \tilde{p}_k^2} \right)^{2+\frac{L'}{2}}, \quad (12)$$

where q_{ij} (\tilde{p}_k) is the momentum of i (k) in the ij (total) center-of-mass frame. The second vertex, $\bar{K}^* \rightarrow \bar{K} \pi$ is common for all the DT diagrams, and is given as

$$c_{\bar{K} \pi, \bar{K}^*} \left(1 t_\pi \frac{1}{2} t_{\bar{K}} \middle| \frac{1}{2} t_{\bar{K}^*} \right) \boldsymbol{\epsilon}_{\bar{K}^*} \cdot (\mathbf{p}_{\bar{K}} - \mathbf{p}_\pi) f_{\bar{K} \pi, \bar{K}^*}^1, \quad (13)$$

with the form factor $f_{ij,k}^L \equiv f_{ij}^L / \sqrt{E_k}$ and

$$f_{ij}^L = \frac{1}{\sqrt{E_i E_j}} \left(\frac{\Lambda^2}{\Lambda^2 + q_{ij}^2} \right)^{2+(L/2)}. \quad (14)$$

The third vertex is either $\Lambda_c \pi \rightarrow \Sigma_c$ or $\Lambda_c \pi \rightarrow \Sigma_c^*$ which are given by

$$c_{\Lambda_c \pi, \Sigma_c} \boldsymbol{\sigma} \cdot \mathbf{p}_\pi f_{\Lambda_c \pi, \Sigma_c}^1, \quad (15)$$

$$c_{\Lambda_c \pi, \Sigma_c^*} \mathbf{S}^\dagger \cdot \mathbf{p}_\pi f_{\Lambda_c \pi, \Sigma_c^*}^1, \quad (16)$$

respectively. We have introduced baryon spin operators \mathbf{S}^\dagger and \mathbf{S} that change a baryon spin as $\frac{1}{2} \rightarrow \frac{3}{2}$ and $\frac{3}{2} \rightarrow \frac{1}{2}$, respectively; they can be expressed with the Pauli matrices as $\mathbf{S} \cdot \mathbf{a} \mathbf{S}^\dagger \cdot \mathbf{b} = \frac{2}{3} \mathbf{a} \cdot \mathbf{b} - \frac{i}{3} \boldsymbol{\sigma} \cdot (\mathbf{a} \times \mathbf{b})$. The fourth vertices cause transitions $\Sigma_c \bar{D}(1/2^-)$, $\Sigma_c^* \bar{D}(3/2^-)$, $\Sigma_c \bar{D}^*(1/2^-)$, $\Sigma_c \bar{D}^*(3/2^-)$, $\Sigma_c^* \bar{D}^*(1/2^-)$, $\Sigma_c^* \bar{D}^*(3/2^-) \rightarrow$

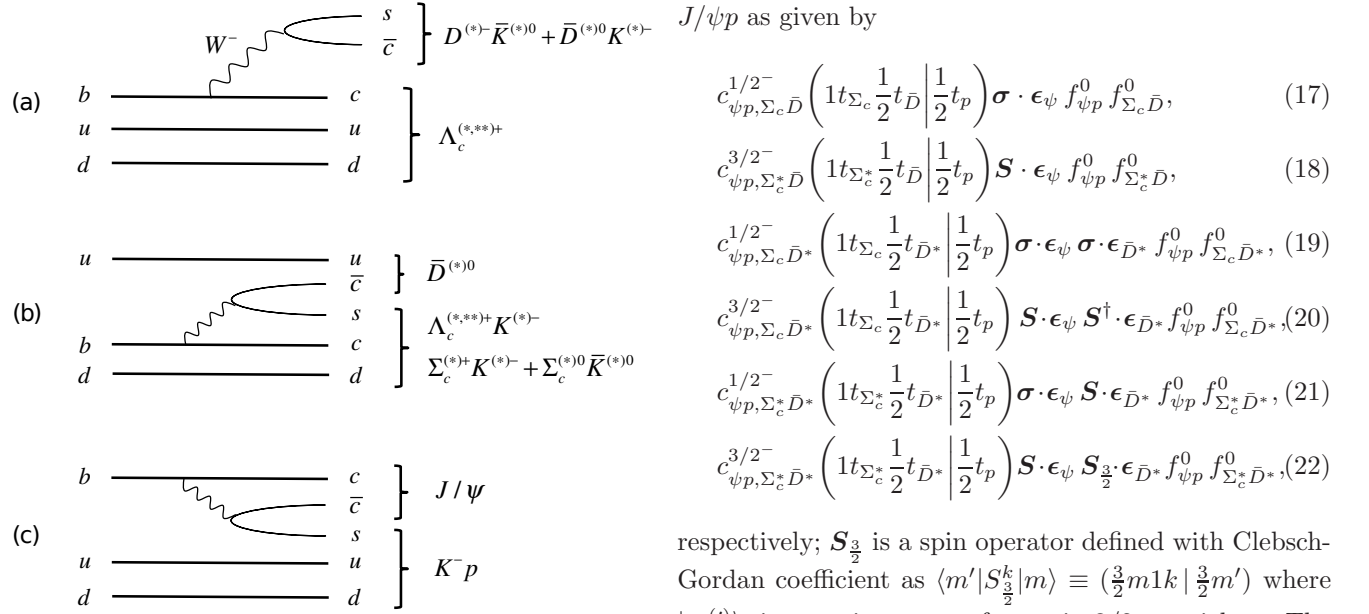


FIG. 4. Quark diagrams for Λ_c^0 decay vertices. (a) Color-favored diagram; (b,c) Color-suppressed diagrams.

respectively; $\mathbf{S}_{\frac{3}{2}}$ is a spin operator defined with Clebsch-Gordan coefficient as $\langle m' | S_{\frac{3}{2}}^k | m \rangle \equiv (\frac{3}{2} m' 1 k | \frac{3}{2} m')$ where $|m^{(\prime)}\rangle$ is a spin state of a spin-3/2 particle. The DT amplitudes including $\Sigma_c^{(*)} \bar{D}^{(*)} (J^P)$, denoted by $A_{\Sigma_c^{(*)} \bar{D}^{(*)} (J^P)}^{\text{DT}}$, are constructed with the above ingredients as

$$A_{\Sigma_c \bar{D} (1/2^-)}^{\text{DT}} = c_{\psi p, \Sigma_c \bar{D}}^{1/2^-} c_{\Lambda_c \pi, \Sigma_c} c_{\bar{K} \pi, \bar{K}^*} c_{\Lambda_c \bar{D} \bar{K}^*, \Lambda_b} \left(1 t_{\Sigma_c} \frac{1}{2} t_{\bar{D}} \left| \frac{1}{2} t_p \right. \right) \left(1 t_\pi \frac{1}{2} t_{\bar{K}} \left| \frac{1}{2} t_{\bar{K}^*} \right. \right) \left(\frac{1}{2} t_{\bar{D}} \frac{1}{2} t_{\bar{K}^*} \left| 00 \right. \right) \int d^3 p_\pi \int d^3 p_{\bar{D}}$$

$$\times \frac{\boldsymbol{\sigma} \cdot \boldsymbol{\epsilon}_\psi \boldsymbol{\sigma} \cdot \mathbf{p}_\pi}{E - E_{\bar{K}} - E_{\Sigma_c} - E_{\bar{D}} + \frac{i}{2} \Gamma_{\Sigma_c}} \frac{\boldsymbol{\sigma} \cdot (\mathbf{p}_{\bar{K}} - \mathbf{p}_\pi)}{E - E_{\bar{K}} - E_\pi - E_{\Lambda_c} - E_{\bar{D}} + i\epsilon} \frac{f_{\psi p}^0 f_{\Sigma_c \bar{D}}^0 f_{\Lambda_c \pi, \Sigma_c}^1 f_{\bar{K} \pi, \bar{K}^*}^1 F_{\bar{K}^* \bar{D} \Lambda_c, \Lambda_b}^{00}}{E - E_{\bar{K}^*} - E_{\Lambda_c} - E_{\bar{D}} + \frac{i}{2} \Gamma_{\bar{K}^*}}, \quad (23)$$

$$A_{\Sigma_c^* \bar{D} (3/2^-)}^{\text{DT}} = c_{\psi p, \Sigma_c^* \bar{D}}^{3/2^-} c_{\Lambda_c \pi, \Sigma_c^*} c_{\bar{K} \pi, \bar{K}^*} c_{\Lambda_c \bar{D} \bar{K}^*, \Lambda_b} \left(1 t_{\Sigma_c^*} \frac{1}{2} t_{\bar{D}} \left| \frac{1}{2} t_p \right. \right) \left(1 t_\pi \frac{1}{2} t_{\bar{K}} \left| \frac{1}{2} t_{\bar{K}^*} \right. \right) \left(\frac{1}{2} t_{\bar{D}} \frac{1}{2} t_{\bar{K}^*} \left| 00 \right. \right) \int d^3 p_\pi \int d^3 p_{\bar{D}}$$

$$\times \frac{\mathbf{S} \cdot \boldsymbol{\epsilon}_\psi \mathbf{S}^\dagger \cdot \mathbf{p}_\pi}{E - E_{\bar{K}} - E_{\Sigma_c^*} - E_{\bar{D}} + \frac{i}{2} \Gamma_{\Sigma_c^*}} \frac{\boldsymbol{\sigma} \cdot (\mathbf{p}_{\bar{K}} - \mathbf{p}_\pi)}{E - E_{\bar{K}} - E_\pi - E_{\Lambda_c} - E_{\bar{D}} + i\epsilon} \frac{f_{\psi p}^0 f_{\Sigma_c^* \bar{D}}^0 f_{\Lambda_c \pi, \Sigma_c^*}^1 f_{\bar{K} \pi, \bar{K}^*}^1 F_{\bar{K}^* \bar{D} \Lambda_c, \Lambda_b}^{00}}{E - E_{\bar{K}^*} - E_{\Lambda_c} - E_{\bar{D}} + \frac{i}{2} \Gamma_{\bar{K}^*}}, \quad (24)$$

$$A_{\Sigma_c^* \bar{D}^* (1/2^-)}^{\text{DT}} = c_{\psi p, \Sigma_c^* \bar{D}^*}^{1/2^-} c_{\Lambda_c \pi, \Sigma_c} c_{\bar{K} \pi, \bar{K}^*} c_{\Lambda_c \bar{D}^* \bar{K}^*, \Lambda_b} \left(1 t_{\Sigma_c^*} \frac{1}{2} t_{\bar{D}^*} \left| \frac{1}{2} t_p \right. \right) \left(1 t_\pi \frac{1}{2} t_{\bar{K}} \left| \frac{1}{2} t_{\bar{K}^*} \right. \right) \left(\frac{1}{2} t_{\bar{D}^*} \frac{1}{2} t_{\bar{K}^*} \left| 00 \right. \right) \int d^3 p_\pi \int d^3 p_{\bar{D}^*}$$

$$\times \frac{\sum_{\epsilon_{\bar{D}^*}} \boldsymbol{\sigma} \cdot \boldsymbol{\epsilon}_\psi \boldsymbol{\sigma} \cdot \boldsymbol{\epsilon}_{\bar{D}^*} \boldsymbol{\sigma} \cdot \mathbf{p}_\pi}{E - E_{\bar{K}} - E_{\Sigma_c} - E_{\bar{D}^*} + \frac{i}{2} \Gamma_{\Sigma_c}} \frac{i \boldsymbol{\sigma} \cdot [(\mathbf{p}_{\bar{K}} - \mathbf{p}_\pi) \times \boldsymbol{\epsilon}_{\bar{D}^*}]}{E - E_{\bar{K}} - E_\pi - E_{\Lambda_c} - E_{\bar{D}^*} + i\epsilon} \frac{f_{\psi p}^0 f_{\Sigma_c^* \bar{D}^*}^0 f_{\Lambda_c \pi, \Sigma_c}^1 f_{\bar{K} \pi, \bar{K}^*}^1 F_{\bar{K}^* \bar{D}^* \Lambda_c, \Lambda_b}^{00}}{E - E_{\bar{K}^*} - E_{\Lambda_c} - E_{\bar{D}^*} + \frac{i}{2} \Gamma_{\bar{K}^*}}, \quad (25)$$

$$A_{\Sigma_c \bar{D}^* (3/2^-)}^{\text{DT}} = c_{\psi p, \Sigma_c \bar{D}^*}^{3/2^-} c_{\Lambda_c \pi, \Sigma_c} c_{\bar{K} \pi, \bar{K}^*} c_{\Lambda_c \bar{D}^* \bar{K}^*, \Lambda_b} \left(1 t_{\Sigma_c} \frac{1}{2} t_{\bar{D}^*} \left| \frac{1}{2} t_p \right. \right) \left(1 t_\pi \frac{1}{2} t_{\bar{K}} \left| \frac{1}{2} t_{\bar{K}^*} \right. \right) \left(\frac{1}{2} t_{\bar{D}^*} \frac{1}{2} t_{\bar{K}^*} \left| 00 \right. \right) \int d^3 p_\pi \int d^3 p_{\bar{D}^*}$$

$$\times \frac{\sum_{\epsilon_{\bar{D}^*}} \mathbf{S} \cdot \boldsymbol{\epsilon}_\psi \mathbf{S}^\dagger \cdot \boldsymbol{\epsilon}_{\bar{D}^*} \boldsymbol{\sigma} \cdot \mathbf{p}_\pi}{E - E_{\bar{K}} - E_{\Sigma_c} - E_{\bar{D}^*} + \frac{i}{2} \Gamma_{\Sigma_c}} \frac{i \boldsymbol{\sigma} \cdot [(\mathbf{p}_{\bar{K}} - \mathbf{p}_\pi) \times \boldsymbol{\epsilon}_{\bar{D}^*}]}{E - E_{\bar{K}} - E_\pi - E_{\Lambda_c} - E_{\bar{D}^*} + i\epsilon} \frac{f_{\psi p}^0 f_{\Sigma_c \bar{D}^*}^0 f_{\Lambda_c \pi, \Sigma_c}^1 f_{\bar{K} \pi, \bar{K}^*}^1 F_{\bar{K}^* \bar{D}^* \Lambda_c, \Lambda_b}^{00}}{E - E_{\bar{K}^*} - E_{\Lambda_c} - E_{\bar{D}^*} + \frac{i}{2} \Gamma_{\bar{K}^*}}, \quad (26)$$

$$A_{\Sigma_c^* \bar{D}^* (1/2^-)}^{\text{DT}} = c_{\psi p, \Sigma_c^* \bar{D}^*}^{1/2^-} c_{\Lambda_c \pi, \Sigma_c^*} c_{\bar{K} \pi, \bar{K}^*} c_{\Lambda_c \bar{D}^* \bar{K}^*, \Lambda_b} \left(1 t_{\Sigma_c^*} \frac{1}{2} t_{\bar{D}^*} \left| \frac{1}{2} t_p \right. \right) \left(1 t_\pi \frac{1}{2} t_{\bar{K}} \left| \frac{1}{2} t_{\bar{K}^*} \right. \right) \left(\frac{1}{2} t_{\bar{D}^*} \frac{1}{2} t_{\bar{K}^*} \left| 00 \right. \right) \int d^3 p_\pi \int d^3 p_{\bar{D}^*}$$

$$\times \frac{\sum_{\epsilon_{\bar{D}^*}} \boldsymbol{\sigma} \cdot \boldsymbol{\epsilon}_\psi \mathbf{S} \cdot \boldsymbol{\epsilon}_{\bar{D}^*} \mathbf{S}^\dagger \cdot \mathbf{p}_\pi}{E - E_{\bar{K}} - E_{\Sigma_c^*} - E_{\bar{D}^*} + \frac{i}{2} \Gamma_{\Sigma_c^*}} \frac{i \boldsymbol{\sigma} \cdot [(\mathbf{p}_{\bar{K}} - \mathbf{p}_\pi) \times \boldsymbol{\epsilon}_{\bar{D}^*}]}{E - E_{\bar{K}} - E_\pi - E_{\Lambda_c} - E_{\bar{D}^*} + i\epsilon} \frac{f_{\psi p}^0 f_{\Sigma_c^* \bar{D}^*}^0 f_{\Lambda_c \pi, \Sigma_c^*}^1 f_{\bar{K} \pi, \bar{K}^*}^1 F_{\bar{K}^* \bar{D}^* \Lambda_c, \Lambda_b}^{00}}{E - E_{\bar{K}^*} - E_{\Lambda_c} - E_{\bar{D}^*} + \frac{i}{2} \Gamma_{\bar{K}^*}}, \quad (27)$$

$$\begin{aligned}
A_{\Sigma_c^* \bar{D}^* (3/2^-)}^{\text{DT}} &= c_{\psi p, \Sigma_c^* \bar{D}^*}^{3/2^-} c_{\Lambda_c \pi, \Sigma_c^*} c_{\bar{K} \pi, \bar{K}^*} c_{\Lambda_c \bar{D}^* \bar{K}^*, \Lambda_b} \left(1 t_{\Sigma_c^*} \frac{1}{2} t_{\bar{D}^*} \left| \frac{1}{2} t_p \right. \right) \left(1 t_{\pi} \frac{1}{2} t_{\bar{K}} \left| \frac{1}{2} t_{\bar{K}^*} \right. \right) \left(\frac{1}{2} t_{\bar{D}^*} \frac{1}{2} t_{\bar{K}^*} \left| 00 \right. \right) \int d^3 p_{\pi} \int d^3 p_{\bar{D}^*} \\
&\times \frac{\sum_{\epsilon_{\bar{D}^*}} \mathbf{S} \cdot \boldsymbol{\epsilon}_{\psi} \mathbf{S}_{3/2} \cdot \boldsymbol{\epsilon}_{\bar{D}^*} \mathbf{S}^{\dagger} \cdot \mathbf{p}_{\pi}}{E - E_{\bar{K}} - E_{\Sigma_c^*} - E_{\bar{D}^*} + \frac{i}{2} \Gamma_{\Sigma_c^*}} \frac{i \boldsymbol{\sigma} \cdot [(\mathbf{p}_{\bar{K}} - \mathbf{p}_{\pi}) \times \boldsymbol{\epsilon}_{\bar{D}^*}]}{E - E_{\bar{K}} - E_{\pi} - E_{\Lambda_c} - E_{\bar{D}^*} + i\epsilon} \frac{f_{\psi p}^0 f_{\Sigma_c^* \bar{D}^*}^0 f_{\Lambda_c \pi, \Sigma_c^*}^1 f_{\bar{K} \pi, \bar{K}^*}^1 F_{\bar{K}^* \bar{D}^* \Lambda_c, \Lambda_b}^{00}}{E - E_{\bar{K}^*} - E_{\Lambda_c} - E_{\bar{D}^*} + \frac{i}{2} \Gamma_{K^*}}, \quad (28)
\end{aligned}$$

where, in each amplitude, the summation over the two charged states with the charge dependent particle masses is implicit; the tiny Γ_{D^*} has been neglected. It is understood that the amplitudes are implicitly sandwiched by initial Λ_b^0 and final p spin state.

Next we present formulas for the one-loop diagrams of Fig. 1(b) including the $\Lambda_c^+ \bar{D}^{*0}(1/2^-)$, $\Lambda_c(2593)^+ \bar{D}^0(1/2^+)$, and $\Lambda_c(2625)^+ \bar{D}^0(3/2^+)$ loops. The initial decay vertices are:

$$c_{\Lambda_c \bar{D}^* \bar{K}, \Lambda_b} \left(\frac{1}{2} t_{\bar{D}^*} \frac{1}{2} t_{\bar{K}} \left| 00 \right. \right) \boldsymbol{\sigma} \cdot \boldsymbol{\epsilon}_{\bar{D}^*} F_{\bar{K} \bar{D}^* \Lambda_c, \Lambda_b}^{00}, \quad (29)$$

$$c_{\Lambda_c^* \bar{D} \bar{K}, \Lambda_b} \left(\frac{1}{2} t_{\bar{D}} \frac{1}{2} t_{\bar{K}} \left| 00 \right. \right) \boldsymbol{\sigma} \cdot (\mathbf{p}_{\bar{D}} - \mathbf{p}_{\bar{K}}) F_{\bar{K} \bar{D} \Lambda_c^*, \Lambda_b}^{10} \quad (30)$$

$$c_{\Lambda_c^{**} \bar{D} \bar{K}, \Lambda_b} \left(\frac{1}{2} t_{\bar{D}} \frac{1}{2} t_{\bar{K}} \left| 00 \right. \right) \mathbf{S}^{\dagger} \cdot (\mathbf{p}_{\bar{D}} - \mathbf{p}_{\bar{K}}) F_{\bar{K} \bar{D} \Lambda_c^{**}, \Lambda_b}^{10}, \quad (31)$$

for $\Lambda_b^0 \rightarrow \Lambda_c^+ \bar{D}^{*0} K^-, \Lambda_c^{*+} \bar{D}^0 K^-,$ and $\Lambda_c^{**+} \bar{D}^0 K^-,$ respectively [$\Lambda_c^* \equiv \Lambda_c(2595)^+, \Lambda_c^{**} \equiv \Lambda_c(2625)^+$]. The coupling constants $c_{\Lambda_c^{(*)} \bar{D}^{(*)} \bar{K}, \Lambda_b}$ are generally complex values. The subsequent interactions for $\Lambda_c^+ \bar{D}^{*0}(1/2^-), \Lambda_c^{*+} \bar{D}^0(1/2^+), \Lambda_c^{**+} \bar{D}^0(3/2^+) \rightarrow J/\psi p$ are

$$c_{\psi p, \Lambda_c \bar{D}^*}^{1/2^-} \boldsymbol{\sigma} \cdot \boldsymbol{\epsilon}_{\psi} \boldsymbol{\sigma} \cdot \boldsymbol{\epsilon}_{\bar{D}^*} f_{\psi p}^0 f_{\Lambda_c \bar{D}^*}^0, \quad (32)$$

$$c_{\psi p, \Lambda_c^* \bar{D}}^{1/2^+} \boldsymbol{\sigma} \cdot \boldsymbol{\epsilon}_{\psi} \boldsymbol{\sigma} \cdot \mathbf{p}_{\psi} f_{\psi p}^1 f_{\Lambda_c^* \bar{D}}^0, \quad (33)$$

$$c_{\psi p, \Lambda_c^{**} \bar{D}}^{3/2^+} \boldsymbol{\sigma} \cdot \boldsymbol{\epsilon}_{\psi} \mathbf{S} \cdot \mathbf{p}_{\psi} f_{\psi p}^1 f_{\Lambda_c^{**} \bar{D}}^0, \quad (34)$$

respectively. The one-loop amplitudes including $\Lambda_c^{(*)} \bar{D}^{(*)0}$, denoted by $A_{\Lambda_c^{(*)} \bar{D}^{(*)}}^{\text{1L}}$, are given with the above ingredients as

$$A_{\Lambda_c \bar{D}^*}^{\text{1L}} = 3 c_{\psi p, \Lambda_c \bar{D}^*}^{1/2^-} c_{\Lambda_c \bar{D}^* \bar{K}, \Lambda_b} \left(\frac{1}{2} t_{\bar{D}^*} \frac{1}{2} t_{\bar{K}} \left| 00 \right. \right) \boldsymbol{\sigma} \cdot \boldsymbol{\epsilon}_{\psi} \int d^3 p_{\bar{D}^*} \frac{f_{\psi p}^0 f_{\Lambda_c \bar{D}^*}^0 F_{\bar{K} \bar{D}^* \Lambda_c, \Lambda_b}^{00}}{E - E_{\bar{K}} - E_{\Lambda_c} - E_{\bar{D}^*} + \frac{i}{2} \Gamma_{D^*}}, \quad (35)$$

$$A_{\Lambda_c^* \bar{D}}^{\text{1L}} = c_{\psi p, \Lambda_c^* \bar{D}}^{1/2^+} c_{\Lambda_c^* \bar{D} \bar{K}, \Lambda_b} \left(\frac{1}{2} t_{\bar{D}} \frac{1}{2} t_{\bar{K}} \left| 00 \right. \right) \boldsymbol{\sigma} \cdot \boldsymbol{\epsilon}_{\psi} \boldsymbol{\sigma} \cdot \mathbf{p}_{\psi} \int d^3 p_{\bar{D}} \boldsymbol{\sigma} \cdot (\mathbf{p}_{\bar{D}} - \mathbf{p}_{\bar{K}}) \frac{f_{\psi p}^1 f_{\Lambda_c^* \bar{D}}^0 F_{\bar{K} \bar{D} \Lambda_c^*, \Lambda_b}^{10}}{E - E_{\bar{K}} - E_{\Lambda_c^*} - E_{\bar{D}} + \frac{i}{2} \Gamma_{\Lambda_c^*}}, \quad (36)$$

$$A_{\Lambda_c^{**} \bar{D}}^{\text{1L}} = c_{\psi p, \Lambda_c^{**} \bar{D}}^{3/2^+} c_{\Lambda_c^{**} \bar{D} \bar{K}, \Lambda_b} \left(\frac{1}{2} t_{\bar{D}} \frac{1}{2} t_{\bar{K}} \left| 00 \right. \right) \boldsymbol{\sigma} \cdot \boldsymbol{\epsilon}_{\psi} \mathbf{S} \cdot \mathbf{p}_{\psi} \int d^3 p_{\bar{D}} \mathbf{S}^{\dagger} \cdot (\mathbf{p}_{\bar{D}} - \mathbf{p}_{\bar{K}}) \frac{f_{\psi p}^1 f_{\Lambda_c^{**} \bar{D}}^0 F_{\bar{K} \bar{D} \Lambda_c^{**}, \Lambda_b}^{10}}{E - E_{\bar{K}} - E_{\Lambda_c^{**}} - E_{\bar{D}} + \frac{i}{2} \Gamma_{\Lambda_c^{**}}}. \quad (37)$$

The resonant $P_c(4440)^+$ amplitude of Fig. 1(c) is given as

$$A_{P_c(4440)}^{1/2^-} = c_{P_c(4440)}^{1/2^-} \frac{\boldsymbol{\sigma} \cdot \boldsymbol{\epsilon}_{\psi} f_{\psi p, P_c}^0 f_{P_c \bar{K}, \Lambda_b}^0}{E - E_{\bar{K}} - E_{P_c} + \frac{i}{2} \Gamma_{P_c}}, \quad (38)$$

for $P_c(4440)^+$ of $J^P = 1/2^-$,

$$\begin{aligned}
A_{P_c(4440)}^{3/2^-} &= c_{P_c(4440)}^{3/2^-} \mathbf{S} \cdot \boldsymbol{\epsilon}_{\psi} \mathbf{S}^{\dagger} \cdot \mathbf{p}_{\bar{K}} \boldsymbol{\sigma} \cdot \mathbf{p}_{\bar{K}} \\
&\times \frac{f_{\psi p, P_c}^0 f_{P_c \bar{K}, \Lambda_b}^2}{E - E_{\bar{K}} - E_{P_c} + \frac{i}{2} \Gamma_{P_c}}, \quad (39)
\end{aligned}$$

for $P_c(4440)^+$ of $J^P = 3/2^-$,

$$\begin{aligned}
A_{P_c(4440)}^{1/2^+} &= c_{P_c(4440)}^{1/2^+} \boldsymbol{\sigma} \cdot \boldsymbol{\epsilon}_{\psi} \boldsymbol{\sigma} \cdot \mathbf{p}_{\psi} \boldsymbol{\sigma} \cdot \mathbf{p}_{\bar{K}} \\
&\times \frac{f_{\psi p, P_c}^1 f_{P_c \bar{K}, \Lambda_b}^1}{E - E_{\bar{K}} - E_{P_c} + \frac{i}{2} \Gamma_{P_c}}, \quad (40)
\end{aligned}$$

for $P_c(4440)^+$ of $J^P = 1/2^+$, and

$$\begin{aligned}
A_{P_c(4440)}^{3/2^+} &= c_{P_c(4440)}^{3/2^+} \boldsymbol{\sigma} \cdot \boldsymbol{\epsilon}_{\psi} \mathbf{S} \cdot \mathbf{p}_{\psi} \mathbf{S}^{\dagger} \cdot \mathbf{p}_{\bar{K}} \\
&\times \frac{f_{\psi p, P_c}^1 f_{P_c \bar{K}, \Lambda_b}^1}{E - E_{\bar{K}} - E_{P_c} + \frac{i}{2} \Gamma_{P_c}}, \quad (41)
\end{aligned}$$

for $P_c(4440)^+$ of $J^P = 3/2^+$.

The direct decays [Fig. 1(d)] may mainly originate from a color-suppressed quark diagram of Fig. 4(c). The corresponding amplitudes can be projected onto the $pJ/\psi(J^P)$ partial waves. Thus we employ a form as fol-

lows:

$$\begin{aligned}
A_{\text{dir}} = & c_{\text{dir}}^{1/2^-} \boldsymbol{\sigma} \cdot \boldsymbol{\epsilon}_\psi F_{\psi p \bar{K}, \Lambda_b}^{00} \\
& + c_{\text{dir}}^{3/2^-} \boldsymbol{S} \cdot \boldsymbol{\epsilon}_\psi \boldsymbol{S}^\dagger \cdot \boldsymbol{p}_{\bar{K}} \boldsymbol{\sigma} \cdot \boldsymbol{p}_{\bar{K}} F_{\psi p \bar{K}, \Lambda_b}^{02} \\
& + c_{\text{dir}}^{1/2^+} \boldsymbol{\sigma} \cdot \boldsymbol{\epsilon}_\psi \boldsymbol{\sigma} \cdot \boldsymbol{p}_\psi \boldsymbol{\sigma} \cdot \boldsymbol{p}_{\bar{K}} F_{\psi p \bar{K}, \Lambda_b}^{11} \\
& + c_{\text{dir}}^{3/2^+} \boldsymbol{\sigma} \cdot \boldsymbol{\epsilon}_\psi \boldsymbol{S} \cdot \boldsymbol{p}_\psi \boldsymbol{S}^\dagger \cdot \boldsymbol{p}_{\bar{K}} F_{\psi p \bar{K}, \Lambda_b}^{11}, \quad (42)
\end{aligned}$$

where $c_{\text{dir}}^{J^P}$ is a (real) coupling constant for the $pJ/\psi(J^P)$ partial wave amplitude; the lowest orbital angular momentum between $pJ/\psi(J^P)$ and K^- is considered. We basically use the common cutoff value for all the vertices discussed above. One exception applies to Eq. (42) where we adjust Λ' of Eq. (12) so that the $M_{J/\psi p}$ distribution from the direct decay amplitude is similar to the phase-space shape.

In numerical calculations, for convenience, all the above amplitudes are evaluated in the $J/\psi p$ center-of-mass frame. With the relevant kinematical factors multiplied, the invariant amplitudes are obtained and are plugged into the Dalitz plot distribution formula. See Appendix B of Ref. [67] for details.

We remark on the choice of the form factors. We choose the dipole form without a particular reason. Other choices such as monopole and exponential forms could also be used, and they should not significantly change the conclusion. This is because the kinematical effects that cause resonancelike structures are not sensitive to the dynamical details such as a particular form of the form factors. We varied the cutoff value over a rather wide range (0.8–2 GeV), and confirmed the stability of the result. This large cutoff variation essentially checked the stability of the result against changing the functional form of the form factors.

The parameter values obtained from fitting and not from fitting the LHCb data [10] are presented in Table I and II, respectively. All coupling parameters for the DT amplitudes have similar magnitudes. Although $c_{\text{dir}}^{3/2^-} = -119.86 \text{ GeV}^{-2}$ seems noticeably larger than the others, this is partly due to the use of a small cutoff value $\Lambda_{\text{dir}}^{3/2^-} = 400 \text{ MeV}$. Here, we remark on possible constraints on the parameters due to the heavy quark spin symmetry (HQSS). The HQSS puts a relation among $c_{\psi p, \Sigma_c^{(*)} \bar{D}^{(*)}}^{J^P}$ as discussed in Ref. [34]. However, this HQSS relation might not strictly constrain the fits in this work. This is because $c_{\psi p, \Sigma_c^{(*)} \bar{D}^{(*)}}^{J^P}$ is always accompanied by $c_{\Lambda_c \bar{D}^{(*)} \bar{K}^*, \Lambda_b}$, and we can determine only their product as seen in the table. The HQSS constraint would be even less restrictive considering that we could have also included: (i) parity-violating initial vertices with more coupling parameters $c_{\Lambda_c \bar{D}^{(*)} \bar{K}^*, \Lambda_b}^{\text{PV}}$; (ii) $\Sigma_c^{(*)} \bar{D}^{(*)} \rightarrow (J/\psi p)_{d\text{-wave}}$ transitions for which the HQSS gives an independent coupling. In the $M_{J/\psi p}$ distribution of $\Lambda_b^0 \rightarrow J/\psi p K^-$, DT mechanisms from these unconsidered vertices would show singular behaviors

similar to the considered DT mechanisms. Thus, in the present analysis, we freely adjust the coupling parameters, and effectively absorb these redundant mechanisms into the parameters of the considered mechanisms. More detailed data are necessary to resolve the redundancy, thereby determining the coupling parameters separately. At this stage, we can examine how the HQSS constrains the fitting parameters.

2. $Y_c \bar{D}^{(*)} \rightarrow J/\psi p$ amplitudes

We describe a single-channel $Y_c \bar{D}^{(*)}$ s -wave scattering (isospin 1/2) with an interaction potential as follows [63]:

$$\begin{aligned}
v_\alpha(p', p) = & \left(T_{Y_c} t'_{Y_c} \frac{1}{2} t'_{\bar{D}^{(*)}} \left| \frac{1}{2} \frac{1}{2} \right. \right) \left(T_{Y_c} t_{Y_c} \frac{1}{2} t_{\bar{D}^{(*)}} \left| \frac{1}{2} \frac{1}{2} \right. \right) \\
& \times f_\alpha^0(p') h_\alpha f_\alpha^0(p), \quad (43)
\end{aligned}$$

where a label α specifies one of $Y_c \bar{D}^{(*)}$ and its J^P ; the isospin of Y_c and its z -component are denoted by T_{Y_c}

TABLE I. Parameter values for the full model ($\Lambda = 1 \text{ GeV}$) obtained from fitting the LHCb data [10]. Each of the parameters is included in the amplitude specified by the equation label in the third column. The parameters above the horizontal line can be arbitrarily scaled by a common overall factor. The parameter value in the last row is shared as $h_{\Lambda_c \bar{D}^{(*)} (1/2^-)} = h_{\Sigma_c^* \bar{D}^{(*)} (1/2^-)} = h_{\Sigma_c^* \bar{D}^{(*)} (3/2^-)}$.

| | | |
|--|------------------|----------|
| $c_{\psi p, \Sigma_c \bar{D}}^{1/2^-} c_{\Lambda_c \bar{D} \bar{K}^*, \Lambda_b}$ | $-2.21 + 4.79 i$ | Eq. (23) |
| $c_{\psi p, \Sigma_c^* \bar{D}}^{3/2^-} c_{\Lambda_c \bar{D} \bar{K}^*, \Lambda_b}$ | $5.59 - 7.49 i$ | Eq. (24) |
| $c_{\psi p, \Sigma_c \bar{D}^*}^{1/2^-} c_{\Lambda_c \bar{D}^* \bar{K}^*, \Lambda_b}$ | $-3.43 - 1.12 i$ | Eq. (25) |
| $c_{\psi p, \Sigma_c \bar{D}^*}^{3/2^-} c_{\Lambda_c \bar{D}^* \bar{K}^*, \Lambda_b}$ | $0.20 + 10.46 i$ | Eq. (26) |
| $c_{\psi p, \Sigma_c^* \bar{D}^*}^{1/2^-} c_{\Lambda_c \bar{D}^* \bar{K}^*, \Lambda_b}$ | $5.00 - 1.40 i$ | Eq. (27) |
| $c_{\psi p, \Sigma_c^* \bar{D}^*}^{3/2^-} c_{\Lambda_c \bar{D}^* \bar{K}^*, \Lambda_b}$ | $12.84 + 9.38 i$ | Eq. (28) |
| $c_{\psi p, \Lambda_c \bar{D}^*}^{1/2^-} c_{\Lambda_c \bar{D}^* \bar{K}, \Lambda_b}$ | $-0.38 - 0.63 i$ | Eq. (35) |
| $c_{\psi p, \Lambda_c^* \bar{D}}^{1/2^+} c_{\Lambda_c^* \bar{D} \bar{K}, \Lambda_b} \text{ (GeV}^{-2}\text{)}$ | $-0.76 - 0.24 i$ | Eq. (36) |
| $c_{\psi p, \Lambda_c^* \bar{D}^*}^{3/2^+} c_{\Lambda_c^* \bar{D}^* \bar{K}, \Lambda_b} \text{ (GeV}^{-2}\text{)}$ | $-0.03 - 1.47 i$ | Eq. (37) |
| $c_{P_c(4440)}^{3/2^-} (\times 10^2)$ | $4.31 - 3.30 i$ | Eq. (39) |
| $c_{\text{dir}}^{1/2^-}$ | 2.01 | Eq. (42) |
| $c_{\text{dir}}^{3/2^-} \text{ (GeV}^{-2}\text{)}$ | -119.86 | Eq. (42) |
| $c_{\text{dir}}^{1/2^+} \text{ (GeV}^{-2}\text{)}$ | 5.69 | Eq. (42) |
| $c_{\text{dir}}^{3/2^+} \text{ (GeV}^{-2}\text{)}$ | 8.23 | Eq. (42) |
| $m_{P_c} \text{ (MeV)}$ | 4443.1 | Eq. (39) |
| $\Gamma_{P_c} \text{ (MeV)}$ | 2.7 | Eq. (39) |
| $h_{\Lambda_c \bar{D}^{(*)} (1/2^-)}$ | 2.50 | Eq. (43) |

TABLE II. Parameter values for the full model ($\Lambda = 1$ GeV) not fitted to the LHCb data [10]. The parameter value in the last row is shared as $h_{\Sigma_c \bar{D}(1/2^-)} = h_{\Sigma_c \bar{D}^*(1/2^-)} = h_{\Sigma_c \bar{D}^*(3/2^-)} = h_{\Sigma_c^* \bar{D}(3/2^-)} = h_{\Lambda_c^* \bar{D}(1/2^+)} = h_{\Lambda_c^* \bar{D}^*(3/2^+)}$.

| | | |
|---------------------------------------|------|-----------------------|
| $c_{\bar{K}\pi, \bar{K}^*}$ | 0.15 | Eqs. (23)-(28) |
| $c_{\Lambda_c \pi, \Sigma_c}$ | 0.46 | Eqs. (23), (25), (26) |
| $c_{\Lambda_c \pi, \Sigma_c^*}$ | 0.87 | Eqs. (24), (27), (28) |
| Λ (MeV) | 1000 | |
| $\Lambda_{\text{dir}}'^{1/2^-}$ (MeV) | 800 | Eq. (42) |
| $\Lambda_{\text{dir}}'^{3/2^-}$ (MeV) | 400 | Eq. (42) |
| $\Lambda_{\text{dir}}'^{1/2^+}$ (MeV) | 800 | Eq. (42) |
| $\Lambda_{\text{dir}}'^{3/2^+}$ (MeV) | 800 | Eq. (42) |
| $h_{\Sigma_c \bar{D}(1/2^-)}$ | -2 | Eq. (43) |

and $t_{Y_c}^{(\prime)}$, respectively. h_α is a coupling constant. The form factor f_α^0 has been defined in Eq. (14). With the above interaction potential, the elastic $Y_c \bar{D}^{(*)}$ scattering amplitude is given as follows:

$$t_\alpha(p', p; E) = \left(T_{Y_c} t_{Y_c}' \frac{1}{2} t_{\bar{D}^{(*)}}' \left| \frac{1}{2} \frac{1}{2} \right. \right) \left(T_{Y_c} t_{Y_c} \frac{1}{2} t_{\bar{D}^{(*)}} \left| \frac{1}{2} \frac{1}{2} \right. \right) \times f_\alpha^0(p') \frac{h_\alpha}{1 - h_\alpha \sigma_\alpha(E)} f_\alpha^0(p), \quad (44)$$

with

$$\sigma_\alpha(E) = \sum_{\text{charge}} \left(T_{Y_c} t_{Y_c}' \frac{1}{2} t_{\bar{D}^{(*)}}' \left| \frac{1}{2} \frac{1}{2} \right. \right)^2 \times \int dq q^2 \frac{[f_\alpha^0(q)]^2}{E - E_{Y_c}(q) - E_{\bar{D}^{(*)}}(q) + \frac{i}{2} \Gamma_{Y_c}} \quad (45)$$

where the summation runs over $\Sigma_c^{(*)+} \bar{D}^{(*)0}$ and $\Sigma_c^{(*)++} \bar{D}^{(*)-}$ for $Y_c = \Sigma_c^{(*)}$; the mass splitting between the different charge states are taken care of; no summation for $Y_c = \Lambda_c^{(*)}$. The tiny Γ_{D^*} has been neglected in Eq. (45). Assuming a perturbative $Y_c \bar{D}^{(*)} \rightarrow J/\psi p$ interaction, we then obtain

$$c_{\psi p, \alpha}^{J P_\alpha} \left(T_{Y_c} t_{Y_c}' \frac{1}{2} t_{\bar{D}^{(*)}}' \left| \frac{1}{2} \frac{1}{2} \right. \right) f_{\psi p}^{L_\alpha} f_\alpha^0(p) [1 - h_\alpha \sigma_\alpha(E)]^{-1}, \quad (46)$$

for the $Y_c \bar{D}^{(*)} (J P_\alpha) \rightarrow J/\psi p$ transition amplitude. Now the DT amplitudes of our full model are obtained by multiplying $[1 - h_\alpha \sigma_\alpha(E)]^{-1}$ with $E = M_{J/\psi p}$ to Eqs. (5) and (23)-(28). The DT amplitudes without this modification are used in the simplified model.

Similarly, the one-loop amplitudes of the full model are obtained by multiplying $[1 - h_\alpha \sigma_\alpha(E)]^{-1}$ to Eqs. (8) and (35)-(37). The one-loop amplitudes without this modification are used in the simplified model.

3. Leading and lower-order singularities of double triangle diagrams

The DT amplitudes of Eqs. (23)-(28) have lower-order singularities in the zero-width limit of unstable particles in the loops. Furthermore, some of the DT amplitudes have leading singularities, considering that the K^* mass can have a range approximately as wide as its width. According to the Coleman-Norton theorem [64], the DT leading singularity occurs only if the loop momenta hit a special kinematical point where: (i) $E = E_1 = E_2 = E_3$ (on-shell condition) with $E_1 \equiv E_{\bar{K}^*} + E_{\Lambda_c} + E_{\bar{D}^{(*)}}$, $E_2 \equiv E_{\bar{K}} + E_\pi + E_{\Lambda_c} + E_{\bar{D}^{(*)}}$, and $E_3 \equiv E_{\bar{K}} + E_{\Sigma_c^{(*)}} + E_{\bar{D}^{(*)}}$; (ii) the internal momenta are all collinear in the center-of-mass frame; (iii) classically allowed kinematics [$\hat{p}_{\bar{K}^*} \cdot \hat{p}_\pi = -1$, $\hat{p}_{\bar{D}^{(*)}} \cdot \hat{p}_{\Sigma_c^{(*)}} = 1$, $v_\pi(\equiv |\mathbf{p}_\pi|/E_\pi) \geq v_{\Lambda_c^+}$, $v_{\bar{D}^{(*)}} \geq v_{\Lambda_c^+}$, and $v_{\Sigma_c^{(*)}} \geq v_{\bar{D}^{(*)}}$ for the case of $\hat{p}_{\Lambda_c} \cdot \hat{p}_{\bar{D}^{(*)}} = 1$]. We examine realistic cases where the above conditions (ii) and (iii) are satisfied but (i) is partly satisfied: (i') $E = E_2 = E_3 \neq E_1$ and $|E - E_1|$ is minimum. In these cases, the DT amplitudes have, at least, the lower-order singularity.

In Table III, we present a set of particle momenta (center-of-mass frame) from Eqs. (23)-(28) that satisfies the above conditions (i'), (ii) and (iii). For this calculation, the K^- momentum is set along the positive axis, and charge dependent masses are averaged. Since $|E_1 - E| \lesssim \Gamma_{K^*}$ indicates the leading singularity, $A_{\Sigma_c \bar{D}}^{\text{DT}}$ and $A_{\Sigma_c \bar{D}^*}^{\text{DT}}$ ($A_{\Sigma_c^* \bar{D}}^{\text{DT}}$ and $A_{\Sigma_c^* \bar{D}^*}^{\text{DT}}$) have the leading (lower-order) singularities. This fact and also a smaller effect from $\Gamma_{\Sigma_c} < \Gamma_{\Sigma_c^*}$ ($\Gamma_{\Sigma_c} \sim 2$ MeV, $\Gamma_{\Sigma_c^*} \sim 15$ MeV) makes $A_{\Sigma_c \bar{D}}^{\text{DT}}$ and $A_{\Sigma_c \bar{D}^*}^{\text{DT}}$ more singular than $A_{\Sigma_c^* \bar{D}}^{\text{DT}}$ and $A_{\Sigma_c^* \bar{D}^*}^{\text{DT}}$ near the $\Sigma_c^{(*)} \bar{D}^{(*)}$ thresholds, as confirmed in Fig. 2.

TABLE III. Particle momenta (center-of-mass frame) that satisfy the conditions (i'), (ii), and (iii) described in the text. All momenta in the table are collinear. $E_1 \equiv E_{\bar{K}^*} + E_{\Lambda_c} + E_{\bar{D}^{(*)}}$. The first column specifies the DT amplitude from Eqs. (23)-(28). The unit of the entries is MeV.

| | $p_{\bar{K}}$ | $p_{\bar{K}^*}$ | p_π | $p_{\Lambda_c^+}$ | $p_{\bar{D}^{(*)}}$ | $p_{\Sigma_c^{(*)}}$ | $E_1 - E$ |
|--|---------------|-----------------|---------|-------------------|---------------------|----------------------|-----------|
| $A_{\Sigma_c \bar{D}}^{\text{DT}}$ | 1061 | 926 | -135 | -471 | -455 | -607 | -76 |
| $A_{\Sigma_c^* \bar{D}}^{\text{DT}}$ | 1006 | 771 | -234 | -346 | -426 | -580 | -211 |
| $A_{\Sigma_c \bar{D}^*}^{\text{DT}}$ | 937 | 807 | -131 | -412 | -395 | -543 | -45 |
| $A_{\Sigma_c^* \bar{D}^*}^{\text{DT}}$ | 879 | 654 | -225 | -266 | -388 | -491 | -164 |

[1] S. Godfrey and N. Isgur, Mesons in a relativized quark model with chromodynamics, Phys. Rev. D **32**, 189

(1985).

- [2] H.-X. Chen, W. Chen, X. Liu, and S.-L. Zhu, The hidden-charm pentaquark and tetraquark states, *Phys. Rep.* **639**, 1 (2016).
- [3] A. Hosaka, T. Iijima, K. Miyabayashi, Y. Sakai, and S. Yasui, Exotic hadrons with heavy flavors: X , Y , Z , and related states, *PTEP* **2016**, 062C01 (2016).
- [4] R.F. Lebed, R.E. Mitchell, and E.S. Swanson, Heavy-Quark QCD Exotica, *Prog. Part. Nucl. Phys.* **93**, 143 (2017).
- [5] A. Esposito, A. Pilloni, and A.D. Polosa, Multiquark Resonances, *Phys. Rept.* **668**, 1 (2017).
- [6] A. Ali, J.S. Lange, and S. Stone, Exotics: Heavy Pentaquarks and Tetraquarks, *Prog. Part. Nucl. Phys.* **97**, 123 (2017).
- [7] F.-K. Guo, C. Hanhart, U.-G. Meißner, Q. Wang, Q. Zhao, and B.-S. Zou, Hadronic molecules, *Rev. Mod. Phys.* **90**, 015004 (2018).
- [8] S.L. Olsen, T. Skwarnicki, and D. Zieminska, Nonstandard heavy mesons and baryons: Experimental evidence, *Rev. Mod. Phys.* **90**, 015003 (2018).
- [9] N. Brambilla, S. Eidelman, C. Hanhart, A. Nefediev, C.-P. Shen, C.E. Thomas, A. Vairo, and C.-Z. Yuan, The XYZ states: Experimental and theoretical status and perspectives, *Phys. Rept.* **873**, 1 (2020).
- [10] R. Aaij et al. (LHCb Collaboration), Observation of a Narrow Pentaquark State, $P_c(4312)^+$, and of the Two-Peak Structure of the $P_c(4450)^+$, *Phys. Rev. Lett.* **122**, 222001 (2019).
- [11] R. Aaij et al. (LHCb Collaboration), Observation of $J/\psi p$ resonances consistent with pentaquark states in $\Lambda_b^0 \rightarrow J/\psi p K^-$ decays, *Phys. Rev. Lett.* **115**, 072001 (2015).
- [12] P.A. Zyla et al. (Particle Data Group), The Review of Particle Physics, *Prog. Theor. Exp. Phys.* **2020**, 083C01 (2020).
- [13] M.-Z. Liu, Y.-W. Pan, F.-Z. Peng, M.S. Sánchez, L.-S. Geng, A. Hosaka, and M.P. Valderrama, Emergence of a complete heavy-quark spin symmetry multiplet: seven molecular pentaquarks in light of the latest LHCb analysis, *Phys. Rev. Lett.* **122**, 242001 (2019).
- [14] C.-W. Xiao, J. Nieves, and E. Oset, Heavy quark spin symmetric molecular states from $\bar{D}^{(*)}\Sigma_c^{(*)}$ and other coupled channels in the light of the recent LHCb pentaquarks, *Phys. Rev. D* **100**, 014021 (2019).
- [15] C.-J. Xiao, Y. Huang, Y.-B. Dong, L.-S. Geng, and D.-Y. Chen, Exploring the molecular scenario of $P_c(4312)$, $P_c(4440)$, and $P_c(4457)$, *Phys. Rev. D* **100**, 014022 (2019).
- [16] Z.-H. Guo and J.A. Oller, Anatomy of the newly observed hidden-charm pentaquark states: $P_c(4312)$, $P_c(4440)$, and $P_c(4457)$, *Phys. Lett. B* **793**, 144 (2019).
- [17] J. He, Study of $P_c(4457)$, $P_c(4440)$, and $P_c(4312)$ in a quasipotential Bethe-Salpeter equation approach, *Eur. Phys. J. C* **79**, 393 (2019).
- [18] F.-K. Guo, H.-J. Jing, U.-G. Meißner, and S. Sakai, Isospin breaking decays as a diagnosis of the hadronic molecular structure of the $P_c(4457)$, *Phys. Rev. D* **99**, 091501(R) (2019).
- [19] H.-X. Chen, W. Chen, and S.-L. Zhu, Possible interpretations of the $P_c(4312)$, $P_c(4440)$, and $P_c(4457)$, *Phys. Rev. D* **100**, 051501(R) (2019).
- [20] R. Chen, Z.-F. Sun, X. Liu, and S.-L. Zhu, Strong LHCb evidence supporting the existence of the hidden-charm molecular pentaquarks, *Phys. Rev. D* **100**, 011502(R) (2019).
- [21] G.-J. Wang, L.-Y. Xiao, R. Chen, X.-H. Liu, X. Liu, and S.-L. Zhu, Probing hidden-charm decay properties of P_c states in a molecular scenario, *Phys. Rev. D* **102**, 036012 (2020).
- [22] T. Gutsche and V.E. Lyubovitskij, Structure and decays of hidden heavy pentaquarks, *Phys. Rev. D* **100**, 094031 (2019).
- [23] B. Wang, L. Meng, and S.-L. Zhu, Hidden-charm and hidden-bottom molecular pentaquarks in chiral effective field theory, *JHEP* **11**, 108 (2019).
- [24] J. He and D.-Y. Chen, Molecular states from $\Sigma_c^{(*)}\bar{D}^{(*)}-\Lambda_c\bar{D}^{(*)}$ interaction, *Eur. Phys. J. C* **79**, 887 (2019).
- [25] Y.-H. Lin and B.-S. Zou, Strong decays of the latest LHCb pentaquark candidates in hadronic molecule pictures, *Phys. Rev. D* **100**, 056005 (2019).
- [26] T.J. Burns and E.S. Swanson, Molecular interpretation of the $P_c(4440)$ and $P_c(4457)$ states, *Phys. Rev. D* **100**, 114033 (2019).
- [27] Y.-J. Xu, C.-Y. Cui, Y.-L. Liu, and M.-Q. Huang, Partial decay widths of $P_c(4312)$ as a $\bar{D}\Sigma_c$ molecular state, *Phys. Rev. D* **102**, 034028 (2020).
- [28] Y. Yamaguchi, H. García-Tecocoatzi, A. Giachino, A. Hosaka, and E. Santopinto, P_c pentaquarks with chiral tensor and quark dynamics, *Phys. Rev. D* **101**, 091502(R) (2020).
- [29] S. Sakai, H.-J. Jing, and F.-K. Guo, Decays of P_c into $J/\psi N$ and $\eta_c N$ with heavy quark spin symmetry, *Phys. Rev. D* **100**, 074007 (2019).
- [30] M.B. Voloshin, Some decay properties of hidden-charm pentaquarks as baryon-meson molecules, *Phys. Rev. D* **100**, 034020 (2019).
- [31] Q. Wu and D.-Y. Chen, Production of P_c states from Λ_b decay, *Phys. Rev. D* **100**, 114002 (2019).
- [32] J.-R. Zhang, Exploring a $\Sigma_c\bar{D}$ state: with focus on $P_c(4312)^+$, *Eur. Phys. J. C* **79**, 1001 (2019).
- [33] H. Xu, Q. Li, C.-H. Chang, and G.-L. Wang, Recently observed P_c as molecular states and possible mixture of $P_c(4457)$, *Phys. Rev. D* **101**, 054037 (2020).
- [34] M.-L. Du, V. Baru, F.-K. Guo, C. Hanhart, U.-G. Meißner, J.A. Oller, and Q. Wang, Interpretation of the LHCb P_c states as hadronic molecules and hints of a narrow $P_c(4380)$, *Phys. Rev. Lett.* **124**, 072001 (2020).
- [35] M.-L. Du, V. Baru, F.-K. Guo, C. Hanhart, U.-G. Meißner, J.A. Oller, and Q. Wang, Revisiting the nature of the P_c pentaquarks, arXiv:2102.07159 [hep-ph].
- [36] C.-W. Xiao, J.-X. Lu, J.-J. Wu, and L.-S. Geng, How to reveal the nature of three or more pentaquark states, *Phys. Rev. D* **102**, 056018 (2020).
- [37] A. Ali and A.Ya. Parkhomenko, Interpretation of the narrow $J/\psi p$ peaks in $\Lambda_b \rightarrow J/\psi p K^-$ decay in the compact diquark model, *Phys. Lett. B* **793**, 365 (2019).
- [38] A. Pimikov, H.-J. Lee, and P. Zhang, Hidden charm pentaquarks with color-octet substructure in QCD Sum Rules, *Phys. Rev. D* **101**, 014002 (2020).
- [39] Z.-G. Wang, Analysis of the $P_c(4312)$, $P_c(4440)$, $P_c(4457)$ and related hidden-charm pentaquark states with QCD sum rules, *Int. J. Mod. Phys. A* **35**, 2050003 (2020).
- [40] R. Zhu, X. Liu, H. Huang, and C.-F. Qiao, Analyzing doubly heavy tetra- and penta-quark states by variational method, *Phys. Lett. B* **797**, 134869 (2019).
- [41] X.-Z. Weng, X.-L. Chen, W.-Z. Deng, and S.-L. Zhu,

- Hidden-charm pentaquarks and P_c states, Phys. Rev. D **100**, 016014 (2019).
- [42] F. Giannuzzi, Heavy pentaquark spectroscopy in the diquark model, Phys. Rev. D **99**, 094006 (2019).
- [43] F. Stancu, Spectrum of the $uudc\bar{c}$ hidden charm pentaquark with an SU(4) flavor-spin hyperfine interaction, Eur. Phys. J. C **79**, 957 (2019).
- [44] Y. Dong, P. Shen, F. Huang, and Z. Zhang, Selected strong decays of pentaquark State $P_c(4312)$ in a chiral constituent quark model, Eur. Phys. J. C **80**, 341 (2020).
- [45] M.I. Eides, V.Yu Petrov, and M.V. Polyakov, New LHCb pentaquarks as hadrocharmonium states, Mod. Phys. Lett. A **35**, 2050151 (2020).
- [46] C. Fernández-Ramírez, A. Pilloni, M. Albaladejo, A. Jackura, V. Mathieu, M. Mikhasenko, J.A. Silva-Castro, and A.P. Szczepaniak, Interpretation of the LHCb $P_c(4312)^+$ Signal, Phys. Rev. Lett. **123**, 092001 (2019).
- [47] S.-Q. Kuang, L.-Y. Dai, X.-W. Kang, and D.-L. Yao, Pole analysis on the hadron spectroscopy of $\Lambda_b^0 \rightarrow J/\psi p K^-$, Eur. Phys. J. C **80**, 433 (2020).
- [48] Q. Wang, X.-H. Liu, and Q. Zhao, Photoproduction of hidden charm pentaquark states $P_c^+(4380)$ and $P_c^+(4450)$, Phys. Rev. D **92**, 034022 (2015).
- [49] V. Kubarovsky and M.B. Voloshin, Formation of hidden-charm penta quarks in photon-nucleon collisions, Phys. Rev. D **92**, 031502(R) (2015).
- [50] M. Karliner and J.L. Rosner, Photoproduction of Exotic Baryon Resonances, Phys. Lett. B **752**, 329 (2016).
- [51] Studying the $P_c(4450)$ resonance in J/ψ photoproduction off protons, A.N. Hiller Blin, C. Fernández-Ramírez, A. Jackura, V. Mathieu, V.I. Mokeev, A. Pilloni, and A.P. Szczepaniak, Phys. Rev. D **94**, 034002 (2016).
- [52] X.-Y. Wang, X.-R. Chen, and J. He, Possibility to study pentaquark states $P_c(4312)$, $P_c(4440)$, and $P_c(4457)$ in $\gamma p \rightarrow J/\psi p$ reaction, Phys. Rev. D **99**, 114007 (2019).
- [53] J.-J. Wu, T.-S.H. Lee, and B.-S. Zou, Nucleon resonances with hidden charm in γp reactions, Phys. Rev. C **100**, 035206 (2019).
- [54] X. Cao and J.-P. Dai, Confronting pentaquark photoproduction with new LHCb observations, Phys. Rev. D **100**, 054033 (2019).
- [55] A. Ali et al. (GlueX Collaboration), First measurement of near-threshold J/ψ exclusive photoproduction off the proton, Phys. Rev. Lett. **123**, 072001 (2019).
- [56] F.-K. Guo, X.-H. Liu, and S. Sakai, Threshold cusps and triangle singularities in hadronic reactions, Prog. Part. Nucl. Phys. **112**, 103757 (2020).
- [57] F.-K. Guo, U.-G. Meißner, W. Wang, and Z. Yang, How to reveal the exotic nature of the $P_c(4450)$, Phys. Rev. D **92**, 071502(R) (2015).
- [58] X.-H. Liu, Q. Wang, and Q. Zhao, Understanding the newly observed heavy pentaquark candidates, Phys. Lett. B **757**, 231 (2016).
- [59] R. J. Eden, P. V. Landshoff, D. I. Olive and J. C. Polkinghorne, The Analytic S-Matrix, (Cambridge University Press, Cambridge, England, 1966).
- [60] R. Aaij et al. (LHCb Collaboration), Evidence for exotic hadron contributions to $\Lambda_b^0 \rightarrow J/\psi p \pi^-$ decays, Phys. Rev. Lett. **117**, 082003 (2016).
- [61] S.X. Nakamura, Triangle singularity appearing as an $X(3872)$ -like peak in $B \rightarrow (J/\psi \pi^+ \pi^-) K \pi$, Phys. Rev. D **102**, 074004 (2020).
- [62] U. Skerbis and S. Prelovsek, Nucleon- J/ψ and nucleon- η_c scattering in P_c pentaquark channels from LQCD, Phys. Rev. D **99**, 094505 (2019).
- [63] S.X. Nakamura, Coupled-channel analysis of $D^+ \rightarrow K^- \pi^+ \pi^+$ decay, Phys. Rev. D **93**, 014005 (2016).
- [64] S. Coleman and R.E. Norton, Singularities in the physical region, Nuovo Cimento **38**, 438 (1965).
- [65] L.D. Landau, On analytic properties of vertex parts in quantum field theory, Nucl. Phys. **13**, 181 (1959).
- [66] X.-K. Dong, F.-K. Guo, and B.-S. Zou, Explaining the Many Threshold Structures in the Heavy-Quark Hadron Spectrum, Phys. Rev. Lett. **126**, 152001 (2021).
- [67] H. Kamano, S.X. Nakamura, T.-S.H. Lee, and T. Sato, Unitary coupled-channels model for three-mesons decays of heavy mesons, Phys. Rev. D **84**, 114019 (2011).